

CHAPTER 11

SOLID PROPELLANT ROCKET FUNDAMENTALS

This is the first of four chapters on solid propellant rockets. It discusses the burning rates, motor performance, grain configurations, and structural analysis. In solid propellant rocket motors—and the word “motor” is as common to solid rockets as the word “engine” is to liquid rockets—the propellant is contained and stored directly in the combustion chamber, sometimes hermetically sealed in the chamber for long-time storage (5 to 20 years). Motors come in many different types and sizes, varying in thrust from about 2 N to over 4 million N (0.4 to over 1 million lbf). Historically, solid propellant rocket motors have been credited with having no moving parts. This is still true of many, but some motor designs include movable nozzles and actuators for vectoring the line of thrust relative to the motor axis. In comparison to liquid rockets, solid rockets are usually relatively simple, are easy to apply (they often constitute most of the vehicle structure), and require little servicing; they cannot be fully checked out prior to use, and thrust cannot usually be randomly varied in flight.

Figures 1-5 and 11-1 show the principal components and features of relatively simple solid propellant rocket motors. The *grain* is the solid body of the hardened *propellant* and typically accounts for 82 to 94% of the total motor mass. Design and stresses of grains are described later in this chapter. Propellants are described in the next chapter. The *igniter* (electrically activated) provides the energy to start the combustion. The grain starts to burn on its exposed inner surfaces. The combustion and ignition of solid propellants are discussed in Chapter 13. This grain configuration has a central cylindrical cavity with eight tapered slots, forming an 8-pointed star. Many grains have slots, grooves, holes, or other geometric features and they alter the initial

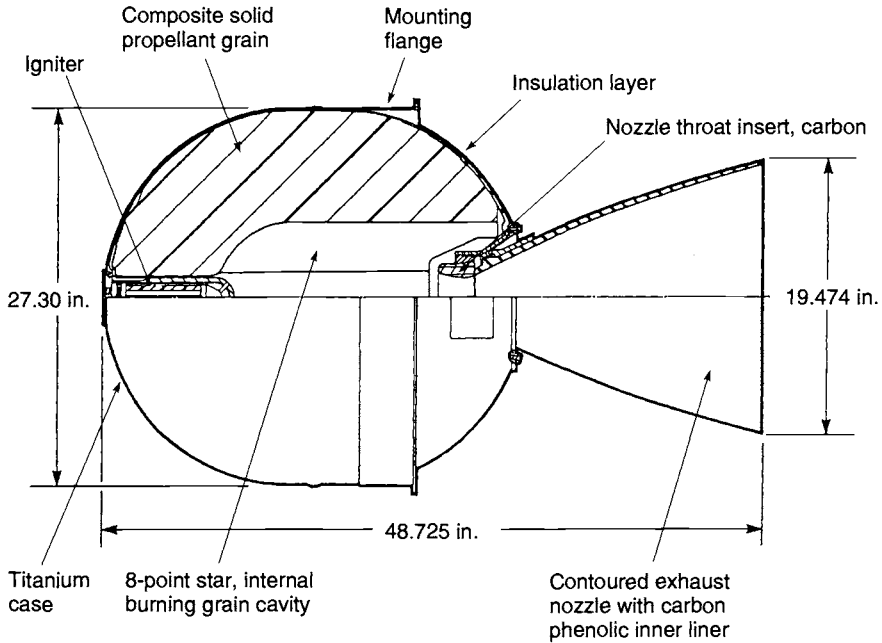


FIGURE 11-1. Cross section of the STARTM 27 rocket motor, which has been used for orbit and satellite maneuvers. It has an altitude thrust of 6000 lbf, nominally burns for 34.4 sec and has an initial mass of 796 lbm. For more data see Table 11-3. (Courtesy of Thiokol Propulsion, a Division of Cordant Technologies.)

burning surface, which determines the initial mass flow and the initial thrust. The hot reaction gases flow along the *perforation* or *port cavity* toward the nozzle. The inner surfaces of the *case* (really a pressure vessel), which are exposed directly to hot gas, have a thermal protection or *insulation layer* to keep the case from becoming too hot, in which case it could no longer carry its pressure and other loads. The case is either made of metal (such as steel, aluminum or titanium) or a composite fiber-reinforced plastic material.

The *nozzle* accelerates the hot gas; it is made of high temperature materials (usually a graphite and/or an ablative material to absorb the heat) to withstand the high temperatures and the erosion. The majority of all solid rockets have a simple fixed nozzle, as shown here, but some nozzles have provision to rotate it slightly so as to control the direction of the thrust to allow vehicle steering. Chapter 14 describes nozzles, cases, insulators, liners, and the design of solid propellant rocket motors.

Each motor is fastened to its vehicle by a thrust-carrying *structure*. In Fig. 11-1 there is a skirt (with a flange) integral with the case; it is fastened to the vehicle.

The subject of thrust vector control, exhaust plumes, and testing are omitted from these four chapters but are treated for both liquid and solid propellant

units in Chapters 16, 18, and 20, respectively. Chapter 17 provides a comparison of the advantages and disadvantages of solid and liquid propellant rocket units. Chapters 3 to 5 are needed as background for these four chapters.

Applications for solid propellant rockets are shown in Tables 1-3, 1-4, and 11-1; each has its own mission requirements and thus propulsion requirements. Figures 11-2, 11-3, and 11-4 illustrate representative designs for some of the major categories of rocket motors listed in Table 11-1: namely, a large booster or second stage, a motor for space flight, and a tactical missile motor. Reference 11-1 is useful for component and design information.

There are several ways for classifying solid propellant rockets. Some are listed in Table 11-2 together with some definitions. Table 11-3 gives characteristics for three specific rocket motors, and from these data one can obtain a feeling for some of the magnitudes of the key parameters. These motors are shown in Figs. 16-5 and 16-9.

Solid propellant rocket motors are being built in approximately 35 different countries today, compared to only three countries about 50 years ago. The technology is well enough understood and disseminated that many companies or government arsenals are now capable of designing developing, and manufacturing solid rockets in several categories.

Almost all rocket motors are used only once. The hardware that remains after all the propellant has been burned and the mission completed—namely, the nozzle, case, or thrust vector control device—is not reusable. In very rare applications, such as the Shuttle solid booster, is the hardware recovered, cleaned, refurbished, and reloaded; reusability makes the design more complex, but if the hardware is reused often enough a major cost saving will result. Unlike some liquid propellant rocket engines, a solid propellant rocket motor and its key components cannot be operationally pretested. As a result, individual motor reliability must be inferred by assuring the structural integrity and verifying manufacturing quality on the entire population of motors.

11.1. PROPELLANT BURNING RATE

The rocket motor's operation and design depend on the combustion characteristics of the propellant, its burning rate, burning surface, and grain geometry. The branch of applied science describing these is known as *internal ballistics*; the effect of grain geometry is treated in Section 11.3.

The burning surface of a propellant grain recedes in a direction essentially perpendicular to the surface. The rate of regression, usually expressed in cm/sec, mm/sec, or in./sec, is the *burning rate* r . In Fig. 11-5 we can visualize the change of the grain geometry by drawing successive burning surfaces with a constant time interval between adjacent surface contours. Figure 11-5 shows this for a two-dimensional grain with a central cylindrical cavity with five slots. Success in rocket motor design and development depends significantly on knowledge of burning rate behavior of the selected propellant under all

(text continues on page 426)

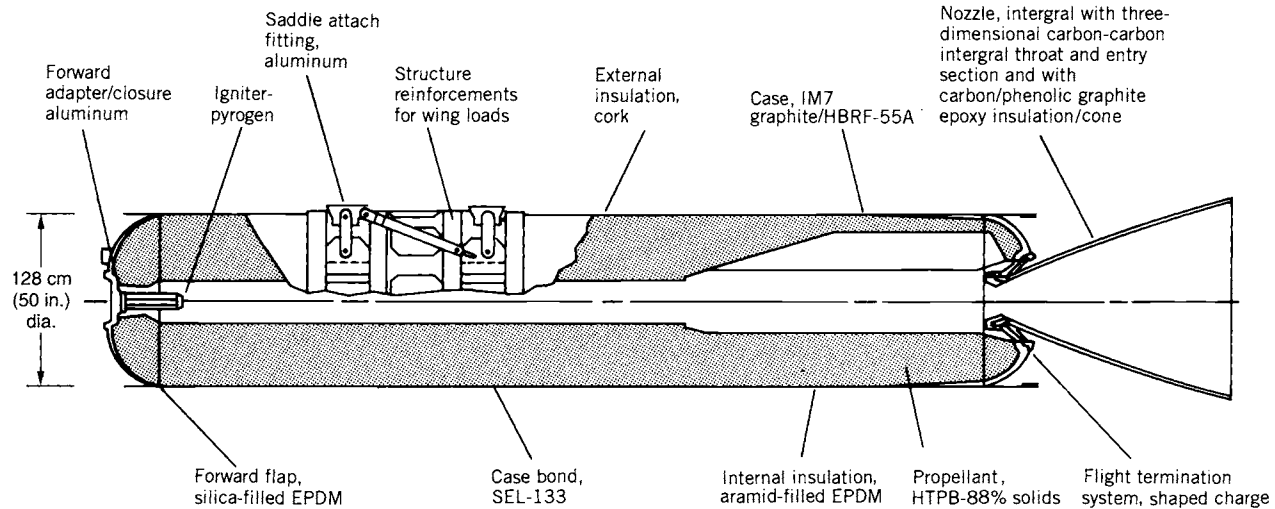


FIGURE 11-2. Booster rocket motor for the Pegasus air-launched three-stage satellite launch vehicle. It has a cylinder grain cavity with fins. The 50 in. diameter case has structural reinforcements to attach the Pegasus vehicle to its launch airplane and also to mount a wing to the case. It produces a maximum vacuum thrust of 726 kN (163,200 lbf) for 68.6 sec, a vacuum specific impulse of 295 sec, with a propellant mass of 15,014 kg and an initial mass of 16,383 kg. (Courtesy of Orbital Sciences, Corp. and Alliant Tech Systems.)

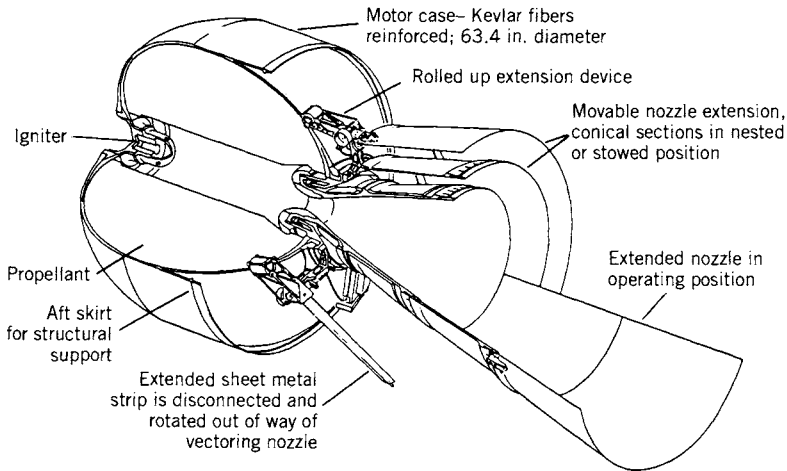


FIGURE 11-3. Inertial upper stage (IUS) rocket motor with an extendible exit cone (EEC). This motor is used for propelling upper launch vehicle stages or spacecraft. The grain is simple (internal tube perforation). With the EEC and a thrust vector control, the motor has a propellant fraction of 0.916. When launched, and while the two lower vehicle stages are operating, the two conical movable nozzle segments are stowed around the smaller inner nozzle segment. Each of the movable segments is deployed in space and moved into its operating position by three identical light-weight, electrically driven actuators. The nozzle area ratio is increased from 49.3 to 181; this improves the specific impulse by about 14 sec. This motor (without the EEC) is described in Table 11-3 and a similar motor is shown in Fig. 16-5. (Courtesy of United Technologies Corp., Chemical Systems.)

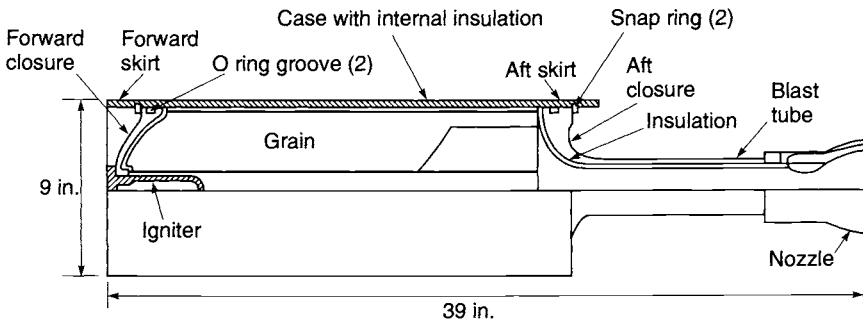


FIGURE 11-4. Simplified cross section through a typical tactical motor. The blast tube allows the grain to be close to the center of gravity of the vehicle; there is very little movement of the center of gravity. The nozzle is at the missile's aft end. The annular space around the blast tube is usually filled with guidance, control, and other non-propulsive equipment. A free-standing grain is loaded before the aft closure is assembled.

TABLE 11-1. Major Application Categories for Solid Propellant Rocket Motors

Category	Application	Typical Characteristics
Large booster and second-stage motors	Space launch vehicles; lower stages of long-range ballistic missiles (see Figs. 11-2 and 14-2)	Large diameter (above 48 in.); L/D of case = 2 to 7; burn time $t = 60$ to 120 sec; low-altitude operations with low nozzle area ratios (6 to 16)
High-altitude motors	Upper stages of multistage ballistic missiles, space launch vehicles; space maneuvers	High-performance propellant; large nozzle area ratio (20 to 200); L/D of case = 1 to 2; burn time $t = 40$ to 120 sec (see Fig. 11-3)
Tactical missiles	<ol style="list-style-type: none"> 1. High acceleration: short-range bombardment, antitank missile 2. Modest acceleration: air-to-surface, surface-to-air, short-range guided surface-to-surface, and air-to-air missiles 	<p>Tube launched, $L/D = 4$ to 13; very short burn time (0.25 to 1 sec); small diameter (2.75 to 18 in.); some are spin stabilized</p> <p>Small diameter (5 to 18 in.); L/D of case = 5 to 10; usually has fins and/or wings; thrust is high at launch and then is reduced (boost-sustain); many have blast tubes (see Fig. 11-4); wide ambient temperature limits: sometimes minimum temperature -65°F or -53°C, maximum temperature $+160^{\circ}\text{F}$ or $+71^{\circ}\text{C}$; usually high acceleration; often low-smoke or smokeless propellant</p>
Ballistic missile defense	Defense against long- and medium-range ballistic missiles	Booster rocket and a small upper maneuverable stage with multiple attitude control nozzles and one or more side or divert nozzles
Gas generator	Pilot emergency escape; push missiles from submarine launch tubes or land mobile cannisters; actuators and valves; short-term power supply; jet engine starter; munition dispersion; rocket turbine drive starter; automotive air bags	Usually low gas temperature ($< 1300^{\circ}\text{C}$); many different configurations, designs, and propellants; purpose is to create high-pressure, energetic gas rather than thrust

TABLE 11-2. Classification of Solid Rocket Motors

Basis of Classification	Examples of Classification
Application	See Table 11-1.
Diameter/Length	0.005–6.6 m or 0.2–260 in.; 0.025 to 45 m or 1 to 1800 in.
Propellant	<i>Composite</i> : Heterogeneous (physical) mixture of powdered metal (fuel), crystalline oxidizer and polymer binder <i>Double-base</i> : Homogeneous mixture (colloidal) of two explosives (usually nitroglycerin in nitrocellulose) <i>Composite-modified double-base</i> : Combines composite and double-base ingredients <i>Gas generator and others</i> : See Chapter 12
Case design	<i>Steel monolithic</i> : One-piece steel case <i>Fiber monolithic</i> : Filament wound (high-strength fibers) with a plastic matrix <i>Segmented</i> : Case (usually steel) and grain are in segments which are transported separately and fastened together at launch site
Grain configuration	<i>Cylindrical</i> : Cylindrically shaped, usually hollow <i>End-burning</i> : Solid cylinder propellant grain <i>Other configurations</i> : See Figs. 11-16 and 11-17
Grain installation	<i>Case-bonded</i> : Adhesion exists between grain and case or between grain and insulation and case; propellant is usually cast into the case <i>Cartridge-loaded</i> : Grain is formed separately from the motor case and then assembled into case
Explosive hazard	<i>Class 1.3</i> : Catastrophic failure shows evidence of burning and explosion, not detonation <i>Class 1.1</i> : Catastrophic failure shows evidence of detonation
Thrust action	<i>Neutral grain</i> : Thrust remains essentially constant during the burn period <i>Progressive grain</i> : Thrust increases with time <i>Regressive grain</i> : Thrust decreases with time <i>Pulse rocket</i> : Two or more independent thrust pulses or burning periods <i>Step-thrust rocket</i> : Usually, two distinct levels of thrust
Toxicity	Toxic and nontoxic exhaust gases

TABLE 11-3. Characteristics of Missile Motor and Space Motor

Characteristic	First Stage Minuteman Missile Motor ^a	Orbus-6 Inertial Upper Stage Motor ^b	STAR TM 27 Apogee Motor ^a
<i>Motor Performance (70°F, sea level)</i>			
Maximum thrust (lbf)	201,500	23,800	6,404 (vacuum)
Burn time average thrust (lbf)	194,600	17,175	6,010 (vacuum)
Action time average thrust (lbf) ^c	176,600	17,180	5,177 (vacuum)
Maximum chamber pressure (psia)	850	839	569
Burn time average chamber pressure (psia) ^c	780	611	552
Action time average chamber pressure (psia) ^c	720	604	502
Burn time/action time (sec) ^c	52.6/61.3	101.0/103.5	34.35/36.93
Ignition delay time (sec)	0.130		0.076
Total impulse (lbf-sec)	10,830,000	1,738,000	213,894
Burn time impulse (lbf-sec)	10,240,000	1,737,000	
Altitude specific impulse (sec)	254	289.6 (vacuum)	290.8 (vacuum)
Temperature limits (°F)	60 to 80	45 to 82	20 to 100
<i>Propellant</i>			
Composition:			
NH ₄ ClO ₄ (%)	70	68	72
Aluminum (%)	16	18	16
Binder and additives (%)	14	14	12
Density (lbm/in. ³)	0.0636	0.0635	0.0641
Burning rate at 1000 psia (in./sec)	0.349	0.276	0.280
Burning rate exponent	0.21	0.3 to 0.45	0.28
Temperature coefficient of pressure (%°F)	0.102	0.09	0.10
Adiabatic flame temperature (°F)	5790	6150	5,909
Characteristic velocity (ft/sec)	5180	5200	5,180
<i>Propellant Grain</i>			
Type	Six-point star	Central perforation	8-point star
Propellant volume (in. ³)	709,400	94,490	11,480
Web (in.)	17.36	24.2	8.17
Web fraction (%)	53.3	77.7	60
Sliver fraction (%)	5.9	0	2.6
Average burning area (in. ²)	38,500	3905	1,378
Volumetric loading (%)	88.7	92.4	
<i>Igniter</i>			
Type	Pyrogen	Pyrogen	Pyrogen
Number of squibs	2	2 through-the bulkhead initiators	2
Minimum firing current (A)	4.9	NA	5.0
<i>Weights (lbf)</i>			
Total	50,550	6515	796.3
Total inert	4719	513	60.6
Burnout	4264	478	53.4

TABLE 11-3. (Continued)

Characteristic	First Stage Minuteman Missile Motor ^a	Orbus-6 Inertial Upper Stage Motor ^b	STAR TM 27 Apogee Motor ^a
Propellant	45,831	6000	735.7
Internal insulation	634	141	12.6
External insulation	309	0	0
Liner	150	Incl. with insulation	0.4
Igniter	26	21	2.9 (empty)
Nozzle	887	143	20.4
Thrust vector control device	Incl. with nozzle	49.4	0
Case	2557	200	23.6
Miscellaneous	156	4	0.7
Propellant mass fraction	0.912	0.921	0.924
<i>Dimensions</i>			
Overall length (in.)	294.87	72.4	48.725
Outside diameter (in.)	65.69	63.3	27.30
<i>Case</i>			
Material	Ladish D6AC steel	Kevlar fibers/epoxy	6 Al-4V titanium
Nominal thickness (in.)	0.148	0.35	0.035
Minimum ultimate strength (psi)	225,000	—	165,000
Minimum yield strength (psi)	195,000	—	155,000
Hydrostatic test pressure (psi)	940	~ 1030	725
Hydrostatic yield pressure (psi)	985	NA	—
Minimum burst pressure, psi	—	1225	76.7
Typical burst pressure, psi	—	> 1350	—
<i>Liner</i>			
Material	Polymeric	HTPB system	TL-H-304
<i>Insulation</i>			
Type	Hydrocarbon- asbestos	Silica-filled EPDM	NA
Density (lbm/in. ³)	0.0394	0.044	
<i>Nozzle</i>			
Number and type	4, movable	Single, flexible	Fixed, contoured
Expansion area ratio	10:1	47.3	48.8/45.94
Throat area (in. ²)	164.2	4.207	5.900
Expansion cone half angle (deg)	11.4	Initial 27.4, final 17.2	Initial 18.9, exit 15.5
Throat insert material	Forged tungsten	Three-dimensional carbon-carbon	3D carbon-carbon
Shell body material	AISI 4130 steel	NA	NA
Exit cone material	NA	Two-dimensional carbon-carbon	Carbon phenolic

^aCourtesy of Thiokol Propulsion, a Division of Cordant Technologies, Inc.

^bCourtesy United Technologies Corp., Chemical Systems; there is also a version Orbus 6-E (see Fig. 11-3) with an extendible, sliding nozzle; it has a specific impulse of 303.8 sec, a total weight of 6604 lb and a burnout weight of 567 lb.

^cBurn time and action time are defined in Fig. 11-13.

NA: not applicable or not available.

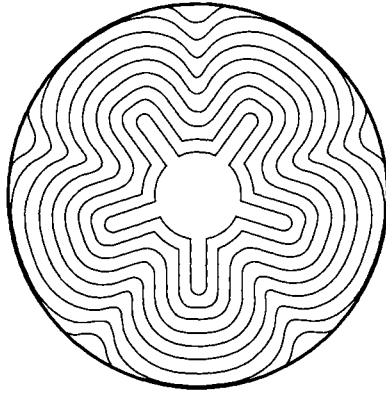


FIGURE 11-5. Diagram of successive burning surface contours, each a fixed small time apart. It shows the growth of the internal cavity. The lengths of these contour lines are roughly the same (within $\pm 15\%$), which means that the burning area is roughly constant.

motor operating conditions and design limit conditions. Burning rate is a function of the propellant composition. For composite propellants it can be increased by changing the propellant characteristics:

1. Add a burning rate *catalyst*, often called burning rate *modifier* (0.1 to 3.0% of propellant) or increase percentage of existing catalyst.
2. *Decrease* the oxidizer particle size.
3. *Increase* oxidizer percentage.
4. Increase the *heat of combustion* of the binder and/or the plasticizer.
5. Imbed *wires* or *metal staples* in the propellant.

Aside from the propellant formulation and propellant manufacturing process, burning rate in a full-scale motor can be increased by the following:

1. Combustion chamber pressure.
2. Initial temperature of the solid propellant prior to start.
3. Combustion gas temperature.
4. Velocity of the gas flow parallel to the burning surface.
5. Motor motion (acceleration and spin-induced grain stress).

Each of these influencing factors will be discussed. The explanation of the behavior of the burning rate with various parameters is largely found in the combustion mechanism of the solid propellant, which is described in Chapter 13. Analytical models of the burning rate and the combustion process exist and are useful for preliminary designs and for extending actual test data; for detail

designs and for evaluation of new or modified propellants, engineers need some actual test data. *Burning rate data* are usually obtained in three ways—namely, from testing by:

1. Standard *strand burners*, often called *Crawford burners*.
2. Small-scale *ballistic evaluation motors*.
3. *Full-scale motors* with good instrumentation.

A strand burner is a small pressure vessel (usually with windows) in which a thin strand or bar of propellant is ignited at one end and burned to the other end. The strand can be inhibited with an external coating so that it will burn only on the exposed cross-sectional surface; chamber pressure is simulated by pressurizing the container with inert gas. The burning rate can be measured by electric signals from embedded wires, by ultrasonic waves, or by optical means (Ref. 11–2). The burning rate measured on strand burners is usually lower than that obtained from motor firing (by 4 to 12%) because it does not truly simulate the hot chamber environment. Also small ballistic evaluation motors usually have a slightly lower burning rate than full-scale larger motors, because of scaling factors. The relationship between the three measured burning rates is determined empirically for each propellant category and grain configuration. Strand-burner data are useful in screening propellant formulations and in quality control operations. Data from full-scale motors tested under a variety of conditions constitute the final proof of burning-rate behavior. Obviously, the strand burner and other substitutes for the full-scale motor must be exploited to explore as many variables as practicable.

During development of a new or modified solid propellant, it is tested extensively or *characterized*. This includes the testing of the burn rate (in several different ways) under different temperatures, pressures, impurities, and conditions. It also requires measurements of physical, chemical, and manufacturing properties, ignitability, aging, sensitivity to various energy inputs or stimuli (e.g., shock, friction, fires), moisture absorption, compatibility with other materials (liners, insulators, cases), and other characteristics. It is a lengthy, expensive, often hazardous program with many tests, samples, and analyses.

The burning rate of propellant in a motor is a function of many parameters, and at any instant governs the mass flow rate \dot{m} of hot gas generated and flowing from the motor (stable combustion):

$$\dot{m} = A_b r \rho_b \quad (11-1)$$

Here A_b is the burning area of the propellant grain, r the burning rate, and ρ_b the solid propellant density prior to motor start. The total mass m of effective propellant burned can be determined by integrating Eq. 11-1:

$$m = \int \dot{m} dt = \rho_b \int A_b r dt \quad (11-2)$$

where A_b and r vary with time and pressure.

Burning Rate Relation with Pressure

Classical equations relating to burning rate are helpful in preliminary design, data extrapolation, and understanding the phenomena; however, analytical modeling and the supportive research have yet to adequately predict the burning rate of a new propellant in a new motor. Elemental laws and equations on burning rate usually deal with the influence of some of the important parameters individually. Unless otherwise stated, burning rate is expressed for 70°F or 294 K propellant (prior to ignition) burning at a reference chamber pressure of 1000 psia or 6.895 MPa.

With many propellants it is possible to approximate the *burning rates* as a function of *chamber pressure*, at least over a limited range of chamber pressures. A log-log plot is shown in Fig. 11-6. For most production-type propellants, this empirical equation is

$$r = ap_1^n \quad (11-3)$$

where r , the burn rate, is usually in centimeters per second or inches per second, and the chamber pressure p_1 is in MPa or psia; a is an empirical constant influenced by ambient grain temperature. This equation applies to all the commonly used double-base, composite, or composite double-base propellants and they are described in the next chapter. Also a is known as the *temperature coefficient* and it is not dimensionless. The *burning rate exponent* n , sometimes called the *combustion index*, is independent of the initial grain temperature and describes the influence of chamber pressure on the burning rate. The change in ambient temperature does not change the chemical energy released in combustion; it merely changes the rate of reaction at which energy is released.

The curves shown in Fig. 11-6 are calculated and are straight lines on a log-log plot; however, many actual burning rate plots deviate somewhat and the actual data have some slight bends in parts of the curve, as seen in Fig. 11-7. For a particular propellant and for wide temperature and pressure limits, the burning rate can vary by a factor of 3 or 4. For all propellants they range from about 0.05 to 75 mm/sec or 0.02 to 3 in./sec; the high values are difficult to achieve, even with considerable burning rate catalyst additives, embedded metal wires, or high pressures (above 14 MPa or 2000 psi). A technology that would give a burning rate of more than 250 mm/sec at a chamber pressure of 1000 psia is desired by motor designers for several applications.

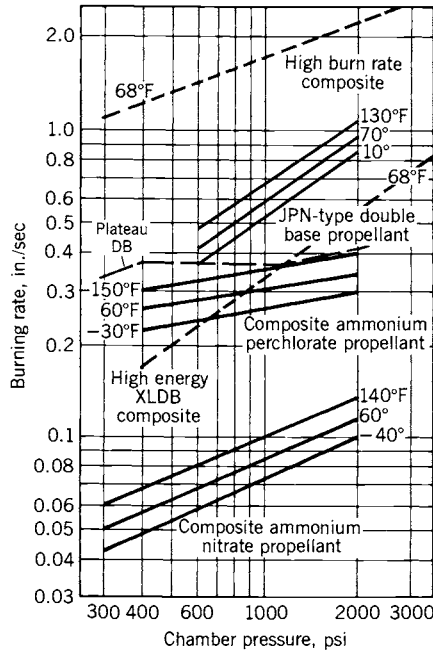


FIGURE 11-6. Plot of the burning rate versus chamber pressure for several typical solid rocket propellants, some at three different temperatures. A particular *double base* plateau propellant shows a constant burning rate over a fairly wide pressure range.

Example 11-1. Tabulate the variation of burning rate with pressure for two propellants with $a_1 = 0.00137$, $n_1 = 0.9$, $a_2 = 0.060$, and $n_2 = 0.4$, with p expressed in pounds per square inch and r in inches per second.

SOLUTION. Use Eq. 11-3 and solve for several conditions, as shown below.

Pressure (psia)	r_1 (in./sec)	r_2 (in./sec)
500	0.367	0.720
1000	0.685	0.95
1500	0.994	1.11
2000	1.28	1.26
2500	1.56	1.33

From inspection of these results and also from Eq. 11-3, it can be seen that the burning rate is very sensitive to the exponent n . For stable operation, n has values greater than 0 and less than 1.0. High values of n give a rapid change of burning rate with pressure. This implies that even a small change in chamber pressure produces substantial changes in the amount of hot gas produced. Most production propellants have a pressure exponent n ranging between 0.2 and 0.6. In practice, as n approaches 1, burning rate and chamber pressure

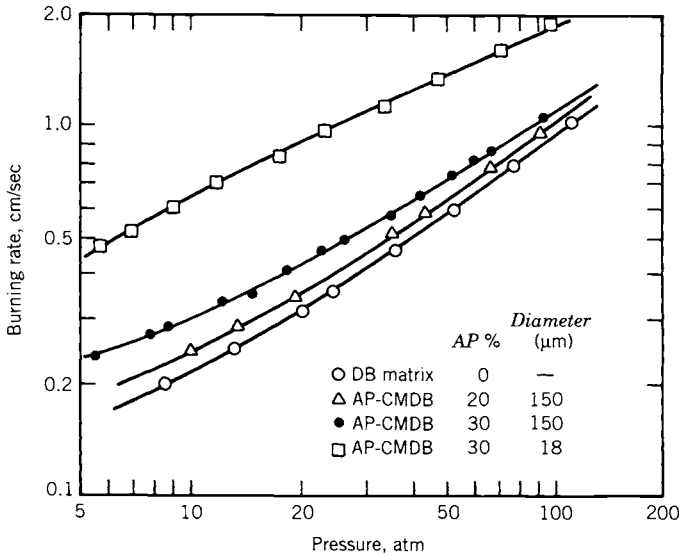


FIGURE 11-7. Measured burning rate characteristics of a double-base (DB) propellant and three composite-modified double-base (CMDB) propellants which contain an increasing percentage of small diameter (159 μm) particles of ammonium perchlorate (AP). When the size of the AP particles is reduced or the percentage of AP is increased, an increase in burning rate is observed. None of these data form straight lines. (Reproduced with permission of the AIAA from Chapter 1 of Ref. 11-3.)

become very sensitive to one another and disastrous rises in chamber pressure can occur in a few milliseconds. When the n value is low and comes closer to zero, burning can become unstable and may even extinguish itself. Some propellants display a negative n which is important for “restartable” motors or gas generators. A propellant having a pressure exponent of zero displays essentially zero change in burning rate over a wide pressure range. *Plateau propellants* are those that exhibit a nearly constant burning rate over a limited pressure range. One is shown with a dashed line in Fig. 11-6; they are relatively insensitive to major changes in chamber pressure for a limited range of pressures. Several double base propellants and a few composite propellants have this desirable plateau characteristic. Table 12-1 lists the nominal burning rate r and the pressure exponent n for several operational (production) propellants.

Burning Rate Relation with Temperature

Temperature affects chemical reaction rates and the initial ambient temperature of a propellant grain prior to combustion influences burning rate, as shown in Figs. 11-6 and 11-8. Common practice in developing and testing larger rocket motors is to “condition” the motor for many hours at a particular temperature

before firing to insure that the propellant grain is uniformly at the desired temperature. The motor performance characteristics must stay within specified acceptable limits. For air-launched missile motors the extremes are usually 219 K (−65°F) and 344 K (160°F). Motors using typical composite propellant experience a 20 to 35% variation in chamber pressure and a 20 to 30% variation in operating time over such a range of propellant temperatures (see Fig. 11-8). In large rocket motors an uneven heating of the grain (e.g., by the sun heating one side) can cause a sufficiently large difference in burning rate so that a slight thrust misalignment can be caused (see Ref. 11-4).

The sensitivity of burning rate to propellant temperature can be expressed in the form of temperature coefficients, the two most common being

$$\sigma_p = \left(\frac{\delta \ln r}{\delta T} \right)_p = \frac{1}{r} \left(\frac{\delta r}{\delta T} \right)_p \quad (11-4)$$

$$\pi_K = \left(\frac{\delta \ln p}{\delta T} \right)_K = \frac{1}{p_1} \left(\frac{\delta p}{\delta T} \right)_K \quad (11-5)$$

with σ_p , known as the *temperature sensitivity of burning rate*, expressed as percent change of burning rate per degree change in propellant temperature at a particular value of chamber pressure, and π_K as the *temperature sensitivity of pressure* expressed as percent change of chamber pressure per degree change in propellant temperature at a particular value of K . Here K is a geometric function, namely the ratio of the burning surface A_b to nozzle throat area A_t .

The coefficient σ_p for a new propellant is usually calculated from strand-burner test data, and π_K from small-scale or full-scale motors. Mathematically,

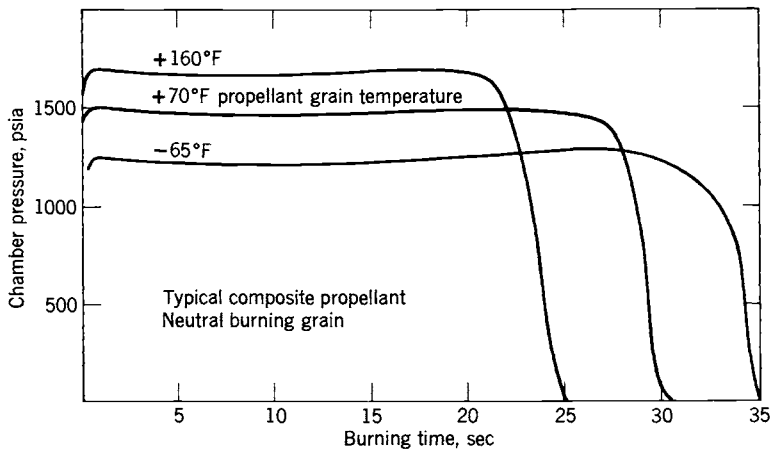


FIGURE 11-8. Effect of propellant temperature on burning time and chamber pressure for a particular motor. The integrated areas under the curves are proportional to the total impulse, which is the same for the three curves.

these coefficients are the partial derivative of the natural logarithm of the burning rate r or the chamber pressure p , respectively, with respect to propellant temperature T . Values for σ_p typically range between 0.001 and 0.009 per degree Kelvin or 0.002 to 0.04 per degree F and for π_K it is 0.067 to 0.278%/°C or 0.12 to 0.50%/°F. With π_K established, the effect of small grain temperature changes on motor chamber pressure is expressed from Eq. 11-5:

$$\Delta p \cong \pi_K p_1 \Delta T \quad (11-6)$$

where p_1 is the reference chamber pressure and Δp is the pressure rise (psia) for a value of ΔT or $T - T_0$.

The values of π_K and σ_p depend primarily on the nature of the propellant burning rate, the composition, and the combustion mechanism of the propellant. It is possible to derive a relationship between the two temperature sensitivities, namely

$$\pi_K = \frac{1}{1-n} \sigma_p \quad (11-7)$$

This formula is usually valid when the three variables are constant over the chamber pressure and temperature range. When substituting the value of r from Eq. 11-3 into Eq. 11-5, the temperature sensitivity σ_p can be also expressed as

$$\sigma_p = \left[\frac{\delta \ln(ap^n)}{\delta T} \right]_p = \frac{1}{a} \frac{da}{dT} \quad (11-8)$$

which then defines σ_p in terms of the changes in the temperature factor a at constant chamber pressure.

It is not simple to predict the motor performance, because of changes in grain temperature and manufacturing tolerances. Reference 11-4 analyses the prediction of burning time.

Example 11-2. For a given propellant with a neutrally burning grain the value of the temperature sensitivity at constant burning area is $\pi_K = 0.005/^\circ\text{F}$ or $0.5\%/^\circ\text{F}$; the value of the pressure exponent n is 0.50. The burning rate r is 0.30 in./sec at 70°F at a chamber pressure of $p_1 = 1500$ psia and an effective nominal burning time of 50 sec. Determine the variation in p_1 and t_b for a change of $\pm 50^\circ\text{F}$ or from $+20^\circ\text{F}$ to $+120^\circ\text{F}$ assuming that the variation is linear.

SOLUTION. First Eq. 11-5 is modified:

$$\pi_K = \Delta p / (p_1 \Delta T) = \Delta p / [1500(\pm 50)] = 0.005$$

Solving, $\Delta p = \pm 375$ psi or a total excursion of about 750 psi or 50% of nominal chamber pressure.

The total impulse or the chemical energy released in combustion stays essentially constant as the grain ambient temperature is changed; only the rate at which it is released is changed. The thrust at high altitude is approximately proportional to the chamber pressure (with A_t and C_F assumed to be essentially constant in the equation $F = C_F p_1 A_t$) and the thrust will change also, about in proportion to the chamber pressure. Then the burning time is approximately

$$t_1 = 50 \times 1500 / (1500 - 375) = 66.7 \text{ sec}$$

$$t_2 = 50 \times 1500 / (1500 + 375) = 40.0 \text{ sec}$$

The time change $66.7 - 40.0 = 26.7$ sec is more than 50% of the nominal burning time. The result would be somewhat similar to what is described in Fig. 11-8.

In this example the variation of chamber pressure affects the thrust and burning time of the rocket motor. The thrust can easily vary by a factor of 2, and this can cause significant changes in the vehicle's flight path when operating with a warm or a cold grain. The thrust and chamber pressure increases are more dramatic if the value of n is increased. The least variation in thrust or chamber pressure occurs when n is small (0.2 or less) and the temperature sensitivity is low.

Burning Enhancement by Erosion

Erosive burning refers to the increase in the propellant burning rate caused by the high-velocity flow of combustion gases over the burning propellant surface. It can seriously affect the performance of solid propellant rocket motors. It occurs primarily in the port passages or perforations of the grain as the combustion gases flow toward the nozzle; it is more likely to occur when the port passage cross-sectional area A is small relative to the throat area A_t with a port-to-throat area ratio of 4 or less. An analysis of erosive burning is given in Ref. 11-5. The high velocity near the burning surface and the turbulent mixing in the boundary layers increase the heat transfer to the solid propellant and thus increase the burning rate. Chapter 10 of Ref. 11-3 surveys about 29 different theoretical analytical treatments and a variety of experimental techniques aimed at a better understanding of erosive burning.

Erosive burning increases the mass flow and thus also the chamber pressure and thrust during the early portion of the burning, as shown in Fig. 11-9 for a particular motor. As soon as the burning enlarges the flow passage (without a major increase in burning area), the port area flow velocity is reduced and erosive burning diminishes until normal burning will again occur. Since propellant is consumed more rapidly during the early erosive burning, there usually is also a reduction of flow and thrust at the end of burning. Erosive burning also causes early burnout of the web, usually at the nozzle end, and exposes the insulation and aft closure to hot combustion gas for a longer period of time; this usually requires more insulation layer thickness (and

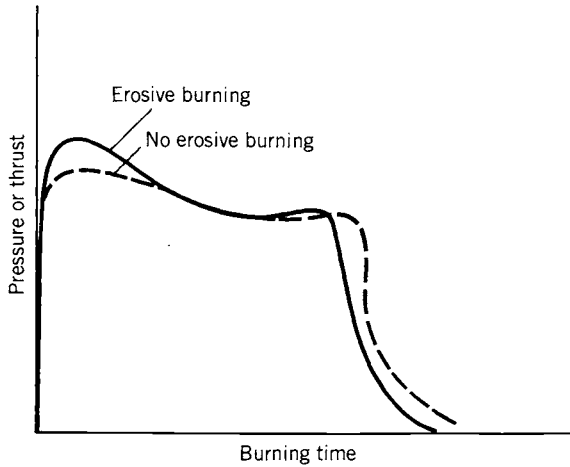


FIGURE 11-9. Typical pressure-time curve with and without erosive burning.

more inert mass) to prevent local thermal failure. In designing motors, erosive burning is either avoided or controlled to be reproducible from one motor to the next.

A relatively simple model for erosive burning, based on heat transfer, was first developed in 1956 by Lenoir and Robillard (Refs. 11-3 and 11-6) and has since been improved and used widely in motor performance calculations. It is based on adding together two burn rates: r_0 , which is primarily a function of pressure and ambient grain temperature (basically Eq. 11-3) without erosion, and r_e , the increase in burn rate due to gas velocity or erosion effects.

$$\begin{aligned}
 r &= r_0 + r_e \\
 &= ap^n + \alpha G^{0.8} D^{-0.2} \exp(-\beta r \rho_b / G)
 \end{aligned}
 \tag{11-9}$$

Here G is the mass flow velocity per unit area in $\text{kg}/\text{m}^2\text{-sec}$, D is a characteristic dimension of the port passage (usually, $D = 4A_p/S$, where A_p is the port area and S is its perimeter), ρ is the density of the unburned propellant (kg/m^3), and α and β are empirically constants. Apparently, β is independent of propellant formulation and has a value of about 53 when r is in m/sec , p_1 is in pascals, and G is in $\text{kg}/\text{m}^2\text{-sec}$. The expression of α was determined from heat transfer considerations to be

$$\alpha = \frac{0.0288 c_p \mu^{0.2} \text{Pr}^{-2/3} T_1 - T_s}{\rho_b c_s T_2 - T_p}
 \tag{11-10}$$

Here c_p is the average specific heat of the combustion gases in kcal/kg-K, μ the gas viscosity in kg/m-sec, Pr the dimensionless Prandtl number ($\mu c_p / \kappa$) based on the molecular properties of the gases, κ the thermal conductivity of the gas, c_s the heat capacity of the solid propellant in kcal/kg-K, T_1 the combustion gas reaction absolute temperature, T_s the solid propellant surface temperature, and T_p the initial ambient temperature within the solid propellant grain.

Figure 11-10 shows the augmentation ratio r/r_0 , or the ratio of the burning rate with and without erosive burning, as a function of gas velocity for two similar propellants, one of which has an iron oxide burn rate catalyst. Augmentation ratios up to 3 can be found in some motor designs. There is a pressure drop from the forward end to the aft end of the port passage, because static pressure energy is converted into kinetic gas energy as the flow is accelerated. This pressure differential during erosive burning causes an extra axial load and deformation on the grain, which must be considered in the stress analysis. The erosion or burn rate augmentation is not the same throughout the length of the port passage. The erosion is increased locally by turbulence if there are discontinuities such as protrusions, edges of inhibitors, structural supports, or gaps between segmented grains.

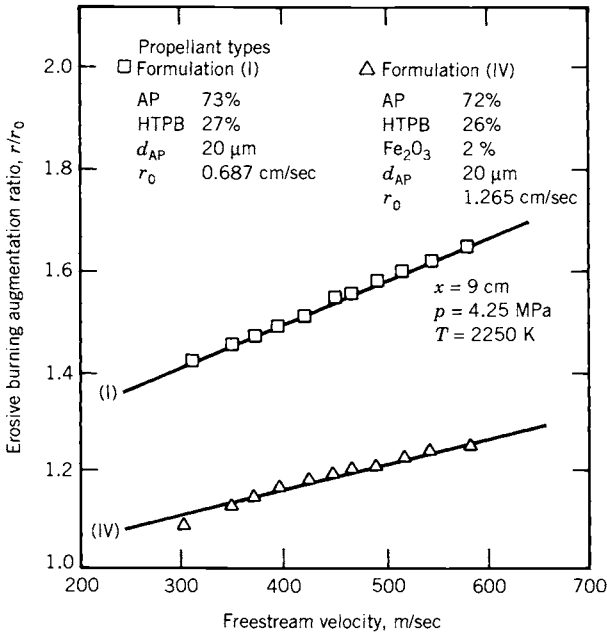


FIGURE 11-10. Effect of gas velocity in the perforation or grain cavity on the erosive burning augmentation factor, which is the burning rate with erosion r divided by the burning rate without erosion r_0 . (Reproduced with permission of the AIAA from Chapter 10 of Ref. 11-3.)

Other Burning Rate Enhancements

Enhancement of burning rate can be expected in vehicles that *spin* the rocket motor about its longitudinal axis (necessary for spin-stabilized flight) or have high *lateral* or *longitudinal acceleration*, as occurs typically in antimissile rockets. This phenomenon has been experienced with a variety of propellants, with and without aluminum fuel, and the propellant formulation is one of the controlling variables (see Fig. 11–11). Whether the acceleration is from spin or longitudinal force, burning surfaces that form an angle of 60 to 90° with the acceleration vector are most prone to burning rate enhancement. For example, spinning cylindrical interal burning grains are heavily affected. The effect of spin on a motor with an operational composite propellant internal burning grain is shown in Fig. 11–12. The accelerated burning behavior of candidate propellants for a new motor design is often determined in small-scale motors, or in a test apparatus which subjects burning propellant to acceleration (Ref. 11–8). The stresses induced by rapid acceleration or rapid chamber pressure rise can cause crack formation (see Refs. 11–9 and 11–10), which exposes additional burning surface.

The burning rate of the propellant in an end-burning grain at a location immediately adjacent to or near the propellant-to-insulation bondline along the case wall, can, depending on the propellant formulation and manufacturing process, be higher than that of the propellant elsewhere in the grain.

The *embedding of wires* or other shapes of good metal heat conductors in the propellant grain increases the burning rate. One technique has several silver wires arranged longitudinally in an end-burning grain (see Ref. 11–11). Depending on wire size and the number of wires per grain cross-sectional area, the burning rate can easily be doubled. Aluminum wires are about half as effective as silver wires. Other forms of heat conductors have been wire

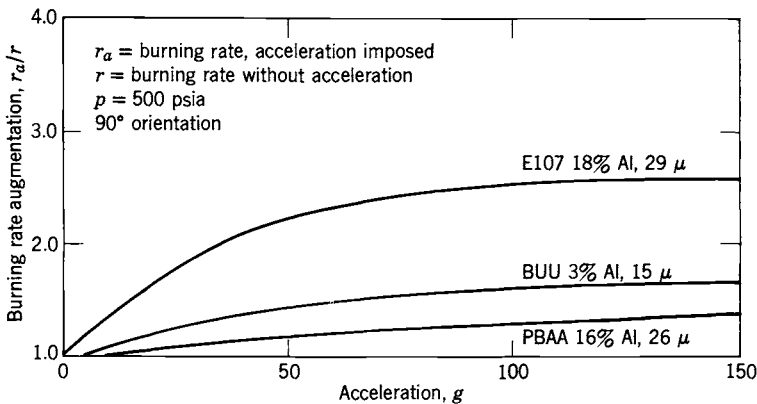


FIGURE 11–11. Acceleration effect on burning rate for three different propellants. (Adapted with permission from Ref. 11–7.)

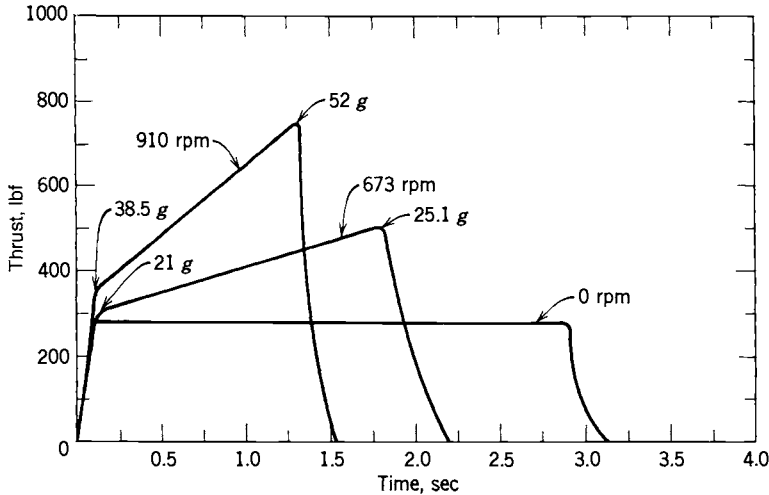


FIGURE 11-12. Effect of axial spin on the thrust–time behavior of a rocket motor with composite propellant using aluminum and PBAN (polybutadiene acrylonitrile) as fuels. (Adapted with permission from Ref. 11-7.)

staples (short bent wires) mixed with the propellant prior to the casting operation.

Intense *radiation emissions* from the hot gases in the grain cavity transfer heat to the burning propellant surfaces. More energetic radiation causes an increase in burning rate. Radiation of the exhaust plume (outside of the nozzle) and the effect of particles in the gas are discussed in Chapter 18.

Combustion instability, also called oscillatory combustion, can affect the burning rate of the propellant because of increased heat-transfer rate, gas velocity, and high pressure. This is discussed in Chapter 13.

11.2. BASIC PERFORMANCE RELATIONS

One basic performance relation is derived from the principle of conservation of matter. The propellant mass burned per unit time has to equal the sum of the change in gas mass per unit time in the combustion chamber grain cavity and the mass flowing out through the exhaust nozzle per unit time.

$$A_b r \rho_b = \frac{d}{dt}(\rho_1 V_1) + A_t p_1 \sqrt{\frac{k}{RT_1} \left(\frac{2}{k+1} \right)^{(k+1)/(k-1)}} \quad (11-11)$$

The term on the left side of the equation gives the mass rate of gas generation from Eq. 11-1. The first term on the right gives the change in propellant mass in the gas volume of the combustion chamber, and the last term gives the

nozzle flow according to Eq. 3-24. The burning rate of the propellant is r ; A_b is the propellant burning area; ρ_b is the solid propellant density; ρ_1 is the chamber gas density; V_1 is the chamber gas cavity volume, which becomes larger as the propellant is expended; A_t is the throat area; p_1 is the chamber pressure; T_1 is the absolute chamber temperature, which is usually assumed to be constant; and k is the specific heat ratio of the combustion gases. During startup the changing mass of propellant in the grain cavity becomes important. The preceding equation can be simplified and is useful in some numerical solutions of transient conditions, such as during start or shutdown.

The value of the burning surface A_b may change with time and is a function of the grain design, as described in Section 11.3. For preliminary performance calculations the throat area A_t is usually assumed to be constant for the total burning duration. For exact performance predictions, it is necessary also to include the erosion of the nozzle material, which causes a small increase in nozzle throat area as the propellant is burned; this nozzle enlargement is described in Chapter 14. The larger value of A_t causes a slight decrease in chamber pressure, burning rate, and thrust.

The gas volume V_1 will increase greatly with burn time. If the gas mass in the motor cavity is small, and thus if the rate of change in this gas mass is small relative to the mass flow through the nozzle, the term $d(\rho_1 V_1)/dt$ can be neglected. Then a relation for steady burning conditions can be obtained from Eqs. 11-3 and 11-11:

$$\begin{aligned} \frac{A_b}{A_t} &= \frac{p_1 \sqrt{k[2/(k+1)]^{(k+1)/(k-1)}}}{\rho_b r \sqrt{RT_1}} = K \\ &= \frac{(p_1)^{1-n} \sqrt{k[2/(k+1)]^{(k+1)/(k-1)}}}{\rho_b a \sqrt{RT_1}} \end{aligned} \quad (11-12)$$

As an approximation, the chamber pressure can be expressed as a function of the area ratio of the burning surface to the nozzle throat cross section for a given propellant:

$$p_1 \sim (A_b/A_t)^{1/(1-n)} = K^{1/(1-n)} \quad (11-13)$$

The ratio of the burning area to the nozzle throat area is an important quantity in solid propellant engineering and is given the separate symbol K . Equations 11-12 and 11-13 show the relation between burning area, chamber pressure, throat area, and propellant properties. For example, this relation permits an evaluation of the variation necessary in the throat area if the chamber pressure (and therefore also the thrust) is to be changed. For a propellant with $n = 0.8$, it can be seen that the chamber pressure would vary as the fifth power of the area ratio K . Thus, small variations in burning surface can have large effects on the internal chamber pressure and therefore also on the

burning rate. The formation of surface cracks in the grain (due to excessive stress) can cause an unknown increase in A_b . A very low value of n is therefore desirable to minimize the effects of small variations in the propellant characteristics or the grain geometry.

Using this equation and the definition of the characteristic velocity c^* from Eq. 3-32, one can write

$$K = A_b/A_t = p_1^{(1-n)}/(a\rho_b c^*) \quad (11-14)$$

Here a and ρ_b are constants and c^* does not really vary much. This can be rewritten

$$p_1 = (Ka\rho_b c^*)^{1/(1-n)} \quad (11-15)$$

The equations above are based on the very simple mathematical dependence of burning rate on chamber pressure. However, for many propellants, this simplification is not sufficiently valid. For accurate evaluation, experimental values must be found.

Those parameters that govern the burning rate and mass discharge rate of motors are called *internal ballistic properties*; they include r , K , σ_p , π_K , and the influences caused by pressure, propellant ingredients, gas velocity, or acceleration. The subsequent solid propellant rocket parameters are *performance parameters*; they include thrust, ideal exhaust velocity, specific impulse, propellant mass fraction, flame temperature, temperature limits, and duration.

The *ideal nozzle exhaust velocity* of a solid propellant rocket is dependent on the thermodynamic theory as given by Eq. 3-15 or 3-16. As explained in Chapter 5, this equation holds only for frozen equilibrium conditions; for shifting equilibrium the exhaust velocity is best defined in terms of the enthalpy drop ($h_1 - h_2$), which can be computed from $v_2 = \sqrt{2(h_1 - h_2)}$. In deriving the exhaust velocity equation, it was assumed that the approach velocity of gases upstream of the nozzle is small and can be neglected. This is true if the port area A_p (the flow area of gases between and around the propellant grains) is relatively large compared to the nozzle throat area A_t . When the port-to-throat-area ratio A_p/A_t is less than about 4, a pressure drop correction must be made to the effective exhaust velocity.

The thrust for solid propellant rockets is given by the identical definitions developed in Chapters 2 and 3, namely, Eqs. 2-14 and 3-29. The *flame or combustion temperature* is a thermochemical property of the propellant formulation and the chamber pressure. It not only affects the exhaust velocity, but also the hardware design, flame radiation emission, materials selection, and the heat transfer to the grain and hardware. In Chapter 5 methods for its calculation are explained. The determination of the nozzle throat area, nozzle expansion area ratio, and nozzle dimensions is discussed in Chapter 3.

The *effective exhaust velocity* c and the *specific impulse* I_s are defined by Eqs. 2-3, 2-4, and 2-6. It is experimentally difficult to measure the instantaneous propellant flow rate or the effective exhaust velocity. However, total impulse and total propellant mass consumed during the test can be measured. The approximate propellant mass is determined by weighing the rocket before and after a test. The effective propellant mass is often slightly less than the total propellant mass, because some grain designs permit small portions of the propellant to remain unburned during combustion, as is explained in a later chapter. Also, a portion of the nozzle and insulation materials erodes and vaporizes during the rocket motor burning and this reduces the final inert mass of the motor and also slightly increases the nozzle mass flow. This explains the difference between the total inert mass and the burnout mass in Table 11-3. It has been found that the *total impulse* can be accurately determined in testing by integrating the area under a thrust time curve. For this reason the average specific impulse is usually calculated from total measured impulse and effective propellant mass. The total impulse I_t is defined by Eq. 2-1 as the integration of thrust F over the operating duration t_b :

$$I_t = \int_0^{t_b} F dt = \bar{F} t_b \quad (11-16)$$

where \bar{F} is an average value of thrust over the burning duration t_b .

The *burning time*, *action time*, and *pressure rise time* at ignition are defined in Fig. 11-13. Time zero is actually when the firing voltage is applied to the ignition squib or prime charge. Visible exhaust gas will actually come out of the rocket nozzle for a period longer than the action time, but the effluent mass flow ahead and behind the action time is actually very small. These definitions are somewhat arbitrary but are commonly in use and documented by standards such as Ref. 2-2.

For flight tests it is possible to derive the instantaneous thrust from the measured flight path acceleration (reduced by an estimated drag) and the estimated instantaneous mass from the chamber pressure measurements, which is essentially proportional to the rocket nozzle mass flow; this gives another way to calculate specific impulse and total impulse.

As explained in Section 3.6, there are at least four values of *specific impulse*: (1) *theoretical specific impulse*, (2) *delivered* or *actual* values as measured from flight tests, static tests, or demonstrations (see Ref. 11-12), (3) *delivered specific impulse at standard or reference conditions*, and (4) the *minimum guaranteed value*. Merely quoting a number for specific impulse without further explanation leaves many questions unanswered. This is similar to the four performance values for liquid propellant engines listed in Section 3.6. Specific impulse as diminished by several losses can be predicted as shown in Ref. 11-13.

Losses include the nozzle inefficiencies due to viscous boundary layer friction and nonaxial flow as described in Chapter 3, thrust vector deflection as described in Chapter 16, residual unburned propellants, heat losses to the walls

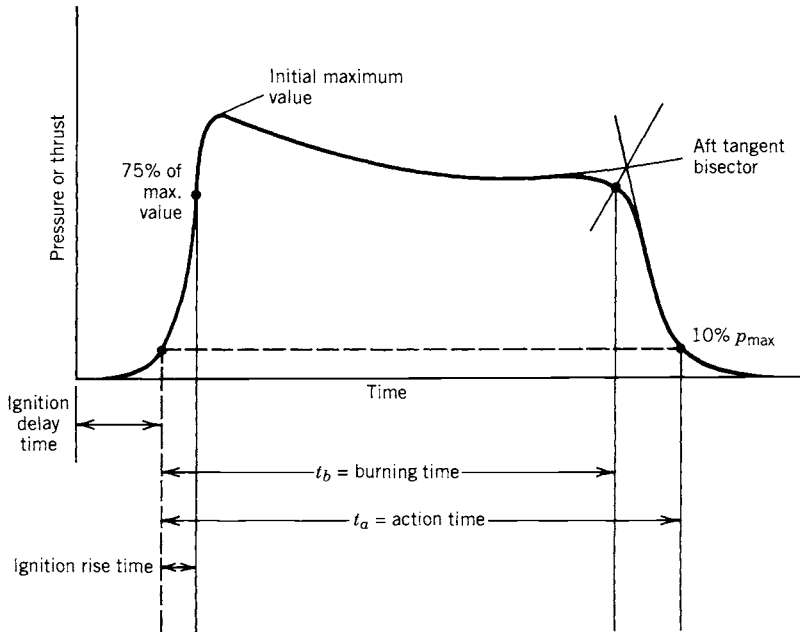


FIGURE 11-13. Definitions of burning time and action time.

or insulators, incomplete combustion, or the presence of solid particles in the gas which need to be accelerated. There are also some performance *gains*; the gases (created by ablation of the ablative nozzle and insulators or the igniter propellants) contribute to an increased mass flow, in many cases also to a somewhat lower average molecular weight of the gas and to a slight reduction of the final inert mass after rocket motor operation.

The *two-phase flow* equations for calculating specific impulse can be solved if the size distribution, shape, and percentage of solid particles in the exhaust gas are known. The assumption of a uniform average spherical particle diameter simplifies the analysis (Ref. 11-13), and this diameter can be estimated from specific impulse measurements on rocket motor tests (Ref. 11-14). Section 3.5 gives a simple theory for two-phase flow of solid particles in a gas flow. Sometimes *density-specific impulse*, the specific gravity of the propellant grain multiplied by specific impulse, is stated as a performance parameter, particularly in rocket motor applications where a compact design is desirable (see Eq. 7-3).

Propellants burn to varying degrees of completeness depending on the fuel, the oxidizer, their ratios, the energy losses, and the environment within the motor. Propellants with nonmetal fuels usually burn with a velocity correction factor of 97 or 98%, as contrasted to 90 to 96% for propellants with aluminum powder as the fuel. The solid particles in the exhaust do not contribute to the gas expansion, require energy to be accelerated, and two-phase flow is less

efficient. However, the addition of the aluminum increases the heat of combustion, the chamber gas temperature, and thus the exhaust velocity or specific impulse. This increase usually outweighs the loss for having to accelerate the small solid aluminum oxide particles.

The *propellant mass fraction* ζ was defined in Eq. 2-8 as $\zeta = m_p/m_0$ and it is directly related to the *motor mass ratio* and therefore also to the flight performance of the vehicle. The initial motor mass m_0 is the sum of the useful solid propellant mass m_p and the non-burning, inert hardware mass of the motor. For a vehicle's propellant mass fraction, the payload mass and the nonpropulsion inert mass (vehicle structure, guidance and control, communications equipment, and power supply) have to be added. A high value of ζ indicates a low inert motor mass, an efficient design of the hardware, and high stresses. This parameter has been used to make approximate preliminary design estimates. It is a function of motor size or mass, thrust level, the nozzle area ratio, and the material used for the case. For very small motors (less than 100 lbm) the value of the propellant fraction is between 0.3 and 0.75. Medium-sized motors ($100 < m_0 < 1000$ lbm) have ζ values between 0.8 and 0.91. For larger motors ($1000 < m_0 < 50,000$ lbm) ζ is between 0.88 and 0.945. A range of values is given for each category, because of the influence of the following other variables. Medium- and large-sized motors with steel cases generally have lower ζ values than those with titanium cases, and their values are lower than for cases made of Kevlar fibers in an epoxy matrix. The highest values are for cases made of graphite or carbon fibers in an epoxy matrix. The ζ values are lower for larger area ratio nozzles and motors with thrust vector control. The STARTM 27 rocket motor, shown in Fig. 11-1 and described in Table 11-3, has a propellant mass fraction of 0.924. This is high for a medium-sized motor with a titanium metal case and a relatively large nozzle exit section.

A number of performance parameters are used to evaluate solid propellant rockets and to compare the quality of design of one rocket with another. The first is the *total-impulse-to-loaded-weight ratio* (I_t/w_G). The loaded weight w_G is the sea-level initial gross weight of propellant and rocket propulsion system hardware. Typical values for I_t/w_G are between 100 and 230 sec, with the higher values representative of high-performance rocket propellants and highly stressed hardware, which means a low inert mass. The total-impulse-to-loaded-weight ratio ideally approaches the value of the specific impulse. When the weight of hardware, metal parts, inhibitors, and so on becomes very small in relation to the propellant weight w_p , then the ratio I_t/w_G approaches I_t/w , which is the definition of the average specific impulse (Eqs. 2-3 and 2-4). The higher the value of I_t/w_G , the better the design of a rocket unit. Another parameter used for comparing propellants is the *volume impulse*; it is defined as the total impulse per unit volume of propellant grain, or I_t/V_b .

The *thrust-to-weight ratio* F/w_G is a dimensionless parameter that is identical to the acceleration of the rocket propulsion system (expressed in multiples of g_0) if it could fly by itself in a gravity-free vacuum; it excludes other vehicle component weights. It is peculiar to the application and can vary from very low

values of less than one g_0 to over 1,000 g_0 for high acceleration applications of solid propellant rocket motors. Some rocket assisted gun munitions have accelerations of 20,000 g_0 .

The *temperature limits* refer to the maximum and minimum storage temperatures to which a motor can be exposed without risk of damage to the propellant grain. They are discussed further in Section 11.4.

Example 11-3. The following requirements are given for a solid propellant rocket motor:

Sea level thrust	2000 lbf average
Duration	10 sec
Chamber pressure	1000 psia
Operating temperature	Ambient (approx. 70°F)
Propellant	Ammonium nitrate-hydrocarbon

Determine the specific impulse, the throat and exit areas, the flow rate, the total propellant weight, the total impulse, the burning area, and an estimated mass assuming moderately efficient design. Properties for this propellant are: $k = 1.26$; $T_1 = 2700^\circ\text{F} = 3160\text{ R}$; $r = 0.10\text{ in./sec}$ at 1000 psia; $c^* = 4000\text{ ft/sec}$; $\rho_b = 0.056\text{ lb/in.}^3$; molecular weight = 22 lbm/lb-mol; gas constant = $1544/22 = 70.2\text{ ft-lbf/lbm-R}$.

SOLUTION. From Figs. 3-4 and 3-6, $C_F = 1.57$ (for $k = 1.26$, with optimum expansion at sea level and a pressure ratio of $1000/14.7 = 68$) and $\epsilon = A_2/A_t = 7.8$. The ideal thrust coefficient has to be corrected for nozzle losses. Assume a correction of 0.98; then $C_F = 0.98 \times 1.57 = 1.54$. The *specific impulse* is (Eq. 3-32).

$$I_s = c^* C_F / g_0 = (4000 \times 1.54) / 32.2 = 191\text{ sec}$$

The *required throat area* is obtained from Eq. 3-31:

$$A_t = F / (p_1 C_F) = 2000 / (1000 \times 1.54) = 1.30\text{ in.}^2$$

The *exit area* is $7.8 \times 1.30 = 10.1\text{ in.}^2$. The *nozzle weight flow rate* is obtained from Eq. 2-5, namely $\dot{w} = F / I_s = 2000 / 191 = 10.47\text{ lbf/sec}$. The *effective propellant weight* for a duration of 10 sec is therefore approximately 105 lbf. Allowing for residual propellant and for inefficiencies on thrust buildup, the *total loaded propellant weight* is assumed to be 4% larger, namely, $105 \times 1.04 = 109\text{ lbf}$.

The *total impulse* is from Eq. 2-2: $I_t = Ft_b = 2000 \times 10 = 20,000\text{ lbf-sec}$. This can also be obtained from $I_t = w \times I_s = 105 \times 191 = 20,000\text{ lbf-sec}$. The propellant burning surface can be found by using Eq. 11-12:

$$\begin{aligned} A_b &= \frac{A_t p_1 \sqrt{k[2/(k+1)]^{(k+1)/(k-1)}}}{\rho_b r \sqrt{RT_1}} \\ &= \frac{1.30 \times 1000}{0.056 \times 0.10} \sqrt{\frac{32.2 \times 1.26}{(1544/22) \times 3160}} (0.885)^{8.7} = 1840\text{ in.}^2 \end{aligned}$$

This result can also be obtained from Eq. 11-11 or 11-14. The ratio is given by

$$K = A_b/A_t = 1840/1.30 = 1415$$

The *loaded gross weight* of the rocket motor (not the vehicle) can only be estimated after a detailed design has been made. However, an approximate guess can be made by choosing a total impulse to weight ratio of perhaps 143.

$$w_G = I_t/(I_t/w_G) = 20,000/143 = 140 \text{ lbf}$$

Because the propellants account for 109 lbf, the hardware parts can be estimated as $140 - 109 = 31$ lbf.

11.3. PROPELLANT GRAIN AND GRAIN CONFIGURATION

The grain is the shaped mass of processed solid propellant inside the rocket motor. The propellant material and geometrical configuration of the grain determine the motor performance characteristics. The propellant grain is a cast, molded, or extruded body and its appearance and feel is similar to that of hard rubber or plastic. Once ignited, it will burn on all its exposed surfaces to form hot gases that are then exhausted through a nozzle. A few rocket motors have more than one grain inside a single case or chamber and very few grains have segments made of different propellant composition (e.g., to allow different burning rates). However, most rockets have a single grain.

There are two methods of holding the grain in the case, as seen in Fig. 11-14. *Cartridge-loaded or freestanding grains* are manufactured separately from the case (by extrusion or by casting into a cylindrical mold or cartridge) and then loaded into or assembled into the case. In *case-bonded grains* the case is used as a mold and the propellant is cast directly into the case and is bonded to the case or case insulation. Free-standing grains can more easily be replaced

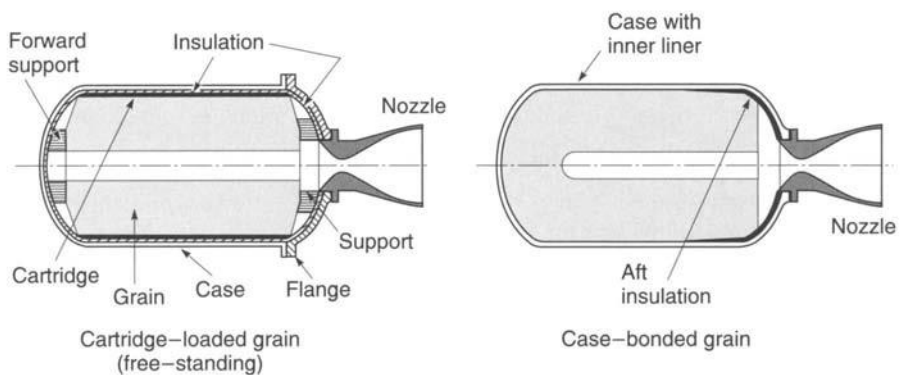


FIGURE 11-14. Simplified schematic diagrams of a free-standing (or cartridge-loaded) and a case-bonded grain.

if the propellant grain has aged excessively. Aging is discussed in the next chapter. Cartridge-loaded grains are used in some small tactical missiles and a few medium-sized motors. They often have a lower cost and are easier to inspect. The case-bonded grains give a somewhat better performance, a little less inert mass (no holding device, support pads, and less insulation), a better volumetric loading fraction, are more highly stressed, and often somewhat more difficult and expensive to manufacture. Today almost all larger motors and many tactical missile motors use case bonding. Stresses in these two types of grains are briefly discussed under structural design in the next section.

Definitions and terminology important to grains include:

Configuration: The shape or geometry of the initial burning surfaces of a grain as it is intended to operate in a motor.

Cylindrical Grain: A grain in which the internal cross section is constant along the axis regardless of perforation shape. (see Fig. 11-3).

Neutral Burning: Motor burn time during which thrust, pressure, and burning surface area remain approximately constant (see Fig. 11-15), typically within about $\pm 15\%$. Many grains are neutral burning.

Perforation: The central cavity port or flow passage of a propellant grain; its cross section may be a cylinder, a star shape, etc. (see Fig. 11-16).

Progressive Burning: Burn time during which thrust, pressure, and burning surface area increase (see Fig. 11-15).

Regressive Burning: Burn time during which thrust, pressure, and burning surface area decrease (see Fig. 11-15).

Sliver: Unburned propellant remaining (or lost—that is, expelled through the nozzle) at the time of web burnout (see sketch in Problem 11-6).

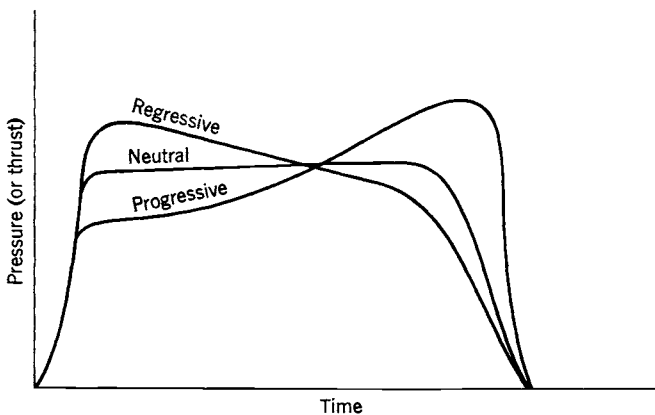


FIGURE 11-15. Classification of grains according to their pressure-time characteristics.

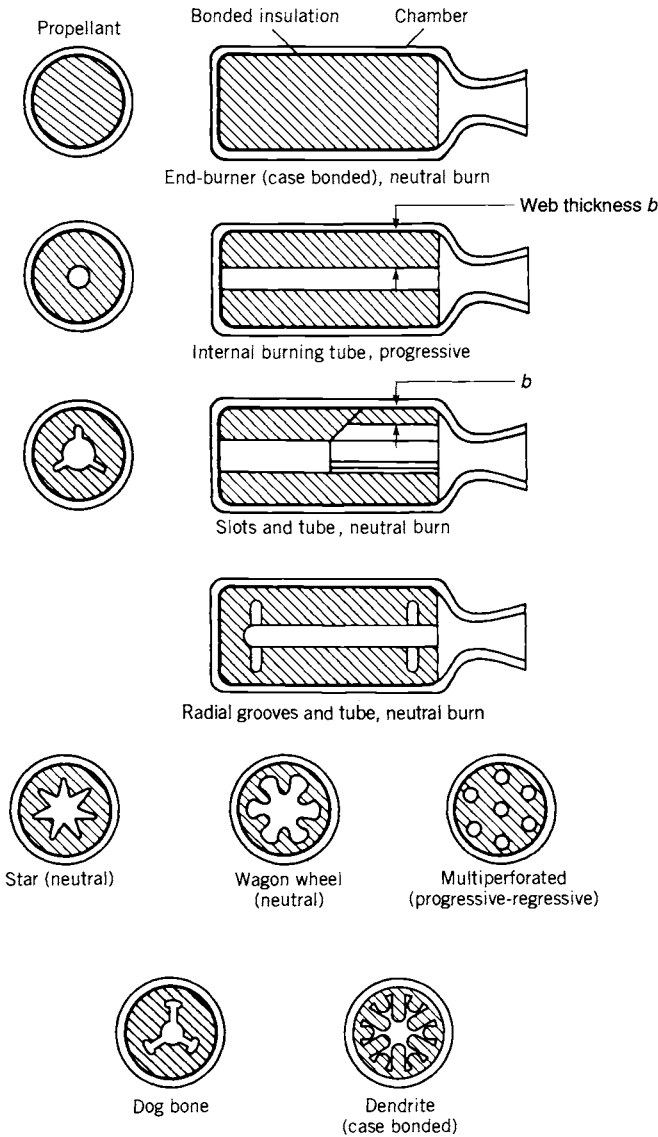


FIGURE 11-16. Simplified diagrams of several grain configurations.

Burning Time, or Effective Burning Time, t_b : Usually, the interval from 10% maximum initial pressure (or thrust) to web burnout, with web burnout usually taken as the aft tangent-bisector point on the pressure-time trace (see Fig. 11-13).

Action Time, t_a : The burning time plus most of the time to burn slivers; typically, the interval between the initial and final 10% pressure (or thrust) points on the pressure-time trace (see Fig. 11-13).

Deflagration Limit: The minimum pressure at which combustion can still be barely self-sustained and maintained without adding energy. Below this pressure the combustion ceases altogether or may be erratic and unsteady with the plume appearing and disappearing periodically.

Inhibitor: A layer or coating of slow- or nonburning material (usually, a polymeric rubber type with filler materials) applied (glued, painted, dipped, or sprayed) to a part of the grain's propellant surface to prevent burning on that surface. By preventing burning on inhibited surfaces the initial burning area can be controlled and reduced. Also called *restrictor*.

Liner: A sticky non-self-burning thin layer of polymeric-type material that is applied to the cases prior to casting the propellant in order to promote good bonding between the propellant and the case or the insulator. It also allows some axial motion between the grain periphery and the case.

Internal Insulator: An internal layer between the case and the propellant grain made of an adhesive, thermally insulating material that will not burn readily. Its purpose is to limit the heat transfer to and the temperature rise of the case during rocket operation. Liners and insulators can be seen in Figs. 11-1, 11-2, 11-4, and 11-14, and are described in Chapter 12.

Web Thickness, b : The minimum thickness of the grain from the initial burning surface to the insulated case wall or to the intersection of another burning surface; for an end-burning grain, b equals the length of the grain (see Fig. 11-16).

Web Fraction, b_f : For a case-bonded internal burning grain, the ratio of the web thickness b to the outer radius of the grain:

$$b_f = b/\text{radius} = 2b/\text{diameter} \quad (11-17)$$

Volumetric Loading Fraction, V_f : The ratio of propellant volume V_b to the chamber volume V_c (excluding nozzle) available for propellant, insulation, and restrictors. Using Eq. 2-4 and $V_b = m/\rho$:

$$V_f = V_b/V_c = I_t/(I_s \rho_b g_0 V_c) \quad (11-18)$$

where I_t is the total impulse, I_s the specific impulse, and ρ_b the propellant density.

A grain has to satisfy several *interrelated requirements*:

1. From the *flight mission* one can determine the *rocket motor requirements*. They have to be defined and known before the grain can be designed. They are usually established by the vehicle designers. This can include total impulse, a desired thrust-time curve and a tolerance thereon, motor mass, ambient temperature limits during storage and operation, available

- vehicle volume or envelope, and vehicle accelerations caused by vehicle forces (vibration, bending, aerodynamic loads, etc.).
2. The *grain geometry* is selected to fit these requirements; it should be compact and use the available volume efficiently, have an appropriate burn surface versus time profile to match the desired thrust–time curve, and avoid or predictably control possible erosive burning. The remaining unburned propellant slivers, and often also the shift of the center of gravity during burning, should be minimized. This selection of the geometry can be complex, and it is discussed in Refs. 11–1 and 11–7 and also below in this section.
 3. The *propellant* is usually selected on the basis of its performance capability (e.g., characteristic velocity), mechanical properties (e.g., strength), ballistic properties (e.g., burning rate), manufacturing characteristics, exhaust plume characteristics, and aging properties. If necessary, the propellant formulation may be slightly altered or “tailored” to fit exactly the required burning time or grain geometry. Propellant selection is discussed in Chapter 12 and in Ref. 11–7.
 4. The *structural integrity* of the grain, including its liner and/or insulator, must be analyzed to assure that the grain will not fail in stress or strain under all conditions of loading, acceleration, or thermal stress. The grain geometry can be changed to reduce excessive stresses. This is discussed in the next section of this chapter.
 5. The complex *internal cavity volume* of perforations, slots, ports, and fins increases with burning time. These cavities need to be checked for resonance, damping, and *combustion stability*. This is discussed in Chapter 13.
 6. The *processing* of the grain and the *fabrication* of the propellant should be simple and low cost (see Chapter 12).

The grain configuration is designed to satisfy most requirements, but sometimes some of these six categories are satisfied only partially. The geometry is crucial in grain design. For a neutral burning grain (approximately constant thrust), for example, the burning surface A_b has to stay approximately constant, and for a regressive burning grain the burning area will diminish during the burning time. From Eqs. 11–3 and 11–14 the trade-off between burning rate and the burning surface area is evident, and the change of burning surface with time has a strong influence on chamber pressure and thrust. Since the density of most modern propellants falls within a narrow range (about 0.066 lbm/in.³ or 1830 kg/m³ +2 to –15%), it has little influence on the grain design.

As a result of motor developments of the past three decades, many *grain configurations* are available to motor designers. As methods evolved for increasing the propellant burning rate, the number of configurations needed decreased. Current designs concentrate on relatively few configurations, since the needs of a wide variety of solid rocket applications can be fulfilled by

combining known configurations or by slightly altering a classical configuration. The trend has been to discontinue configurations that give weak grains which can form cracks, produce high sliver losses, have a low volumetric loading fraction, or are expensive to manufacture.

The effect of propellant burning on surface area is readily apparent for simple geometric shapes such as rods, tubes, wedges, and slots, as shown in the top four configurations of Fig. 11–16. Certain other basic surface shapes burn as follows: external burning rod—regressive; external burning wedge—regressive. Most propellant grains combine two or more of these basic surfaces to obtain the desired burning characteristic. The star perforation, for example, combines the wedge and the internal burning tube. Figure 11–17 indicates typical single grains with combinations of two basic shapes. The term *conocyl* is a contraction of the words *cone* and *cylinder*.

Configurations that combine both radial and longitudinal burning, as does the internal–external burning tube without restricted ends, are frequently referred to as “three-dimensional grains” even though all grains are geometrically three-dimensional. Correspondingly, grains that burn only longitudinally

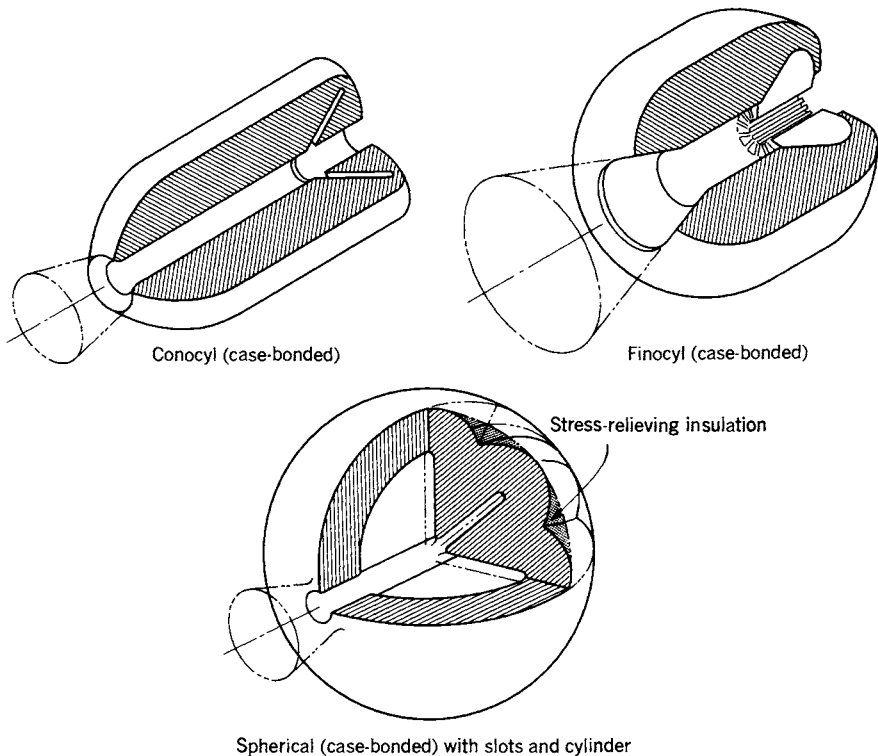


FIGURE 11–17. Typical common grain configurations using combinations of two basic shapes for the grain cavity.

or only radially are “two-dimensional grains.” Grain configurations can be classified according to their web fraction b_f , their length-to-diameter ratio L/D , and their volumetric loading fraction V_f . These three dependent variables are often used in selecting a grain configuration in the preliminary design of a motor for a specific application. Obvious overlap of characteristics exists with some of the configurations, as given in Table 11-4 and shown by simple sketches in Fig. 11-16. The configurations listed above the line in the table are common in recent designs. The bottom three were used in earlier designs and usually are more difficult to manufacture or to support in a case. The end burner has the highest volumetric loading fraction, the lowest grain cavity volume for a given total impulse, and a relatively low burning area or thrust with a long duration. The internal burning tube is relatively easy to manufacture and is neutral burning with unrestricted ends of $L/D \approx 2$. By adding fins or cones (see Fig. 11-17) this configuration works for $2 < L/D < 4$. The star configuration is ideal for web fractions of 0.3 to 0.4; it is progressive above 0.4, but can be neutralized with fins or slots. The wagon wheel is structurally superior to the star shape around 0.3 and is necessary at a web fraction of 0.2 (high thrust and short burn time). Dendrites are used in the lowest web fraction when a relatively large burning area is needed (high thrust and short duration), but stresses may be high. Although the limited number of configurations given in this table may not encompass all the practical possibilities for fulfilling a nearly constant thrust-time performance requirement, combinations of these features should be considered to achieve a neutral pressure-time trace and high volumetric loading before a relatively unproven configuration is accepted. The capabilities of basic configurations listed in these tables can be

TABLE 11-4. Characteristics of Several Grain Configurations

Configuration	Web Fraction	L/D ratio	Volumetric Fraction	Pressure-time Burning Characteristics	C.G. shift
End burner	> 1.0	NA	0.90-0.98	Neutral	Large
Internal burning tube (including slotted tube, trumpet, conocyl, finocyl)	0.5-0.9	1-4	0.80-0.95	Neutral ^a	Small to moderate
Segmented tube (large grains)	0.5-0.9	> 2	0.80-0.95	Neutral	Small
Internal star ^b	0.3-0.6	NA	0.75-0.85	Neutral	Small
Wagon Wheel ^b	0.2-0.3	NA	0.55-0.70	Neutral	Small
Dendrite ^b	0.1-0.2	1-2	0.55-0.70	Neutral	Small
Internal-external burning tube	0.3-0.5	NA	0.75-0.85	Neutral	Small
Rod and tube	0.3-0.5	NA	0.60-0.85	Neutral	Small
Dog bone ^b	0.2-0.3	NA	0.70-0.80	Neutral	Small

^aNeutral if ends are unrestricted, otherwise progressive.

^bHas up to 4 or sometimes 8% sliver mass and thus a gradual thrust termination.

NA: not applicable or not available.

extended by alterations. The movement of the center of gravity influences the flight stability of the vehicle. Relative values of this CG shift are also shown in Table 11-4. Most solid propellant manufacturers have specific approaches and sophisticated computer programs for analyzing and optimizing grain geometry alternatives and permitting burn surface and cavity volume analysis. See Refs. 11-15 and 11-16 and Chapters 8 and 9 of Ref. 11-1.

The *end burning grain* (burning like a cigarette) is unique; it burns solely in the axial direction and maximizes the amount of propellant that can be placed in a given cylindrical motor case. In larger motors (over 0.6 m diameter) these end burners show a progressive thrust curve. Figure 11-18 shows that the burning surface soon forms a conical shape, causing a rise in pressure and thrust. Although the phenomenon is not fully understood, two factors contribute to higher burning rate near the bondline: chemical migration of the burning rate catalyst into and towards the bondline, and local high propellant stresses and strains at the bond surface, creating local cracks (Ref. 11-17).

Rockets used in air-launched or certain surface-launched missile applications, weather rockets, certain anti-aircraft or antimissile rockets, and other tactical applications actually benefit by reducing the thrust with burn time. A high thrust is desired to apply initial acceleration, but, as propellant is consumed and the vehicle mass is reduced, a decrease in thrust is desirable; this limits the maximum acceleration on the rocket-propelled vehicle or its sensitive payload, often reduces the drag losses, and usually permits a more effective flight path. Therefore, there is a benefit to vehicle mass, flight performance, and cost in having a higher initial thrust during the *boost phase* of the flight, followed by a lower thrust (often 10 to 30% of boost thrust) during the *sustaining phase* of the powered flight. Figure 11-19 shows grains which give two or more discrete thrust periods in a single burn operation. The configurations are actually combinations of the configurations listed in Table 11-4.

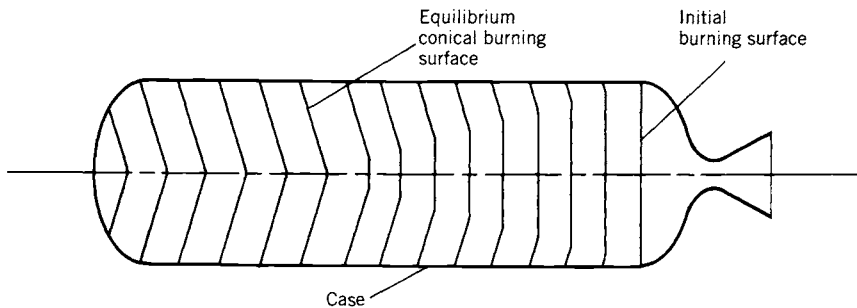


FIGURE 11-18. Schematic diagram of end-burning grain coning effect. In larger sizes (above approximately 0.5 m diameter) the burning surface does not remain flat and perpendicular to the motor axis, but gradually assumes a conical shape. The lines in the grain indicate successively larger-area burning surface contours.

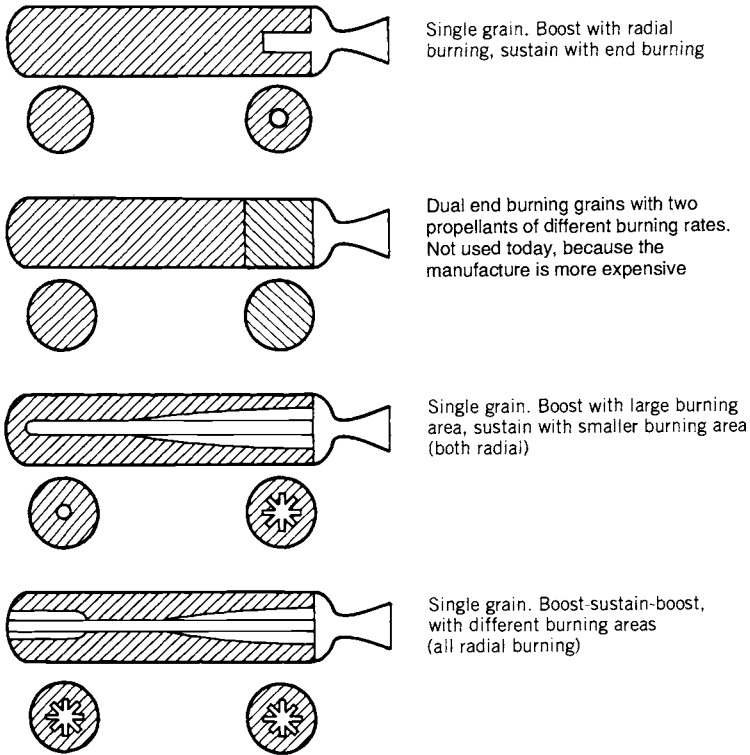


FIGURE 11-19. Several simplified schematic diagrams of grain configurations for an initial period of high thrust followed by a lower-thrust period.

In a single-propellant dual-thrust level solid rocket motor, factors relating to the sustain portion usually dominate in the selection of the propellant type and grain configuration if most of the propellant volume is used during the longer sustain portion.

A *restartable rocket motor* has advantages in a number of tactical rocket propulsion systems used for aircraft and missile defense applications. Here two (or sometimes three) grains are contained inside the same case, each with its own igniter. The grains are physically separated typically by a structural bulkhead or by an insulation layer. One method for accomplishing this is shown in Fig. 11-20. The timing between thrust periods (sometimes called *thrust pulses*) can be controlled and commanded by the missile guidance system, so as to change the trajectory in a nearly optimum fashion and minimize the flight time to target. The separation mechanism has to prevent the burning-hot pressurized gas of the first grain from reaching the other grain and causing its inadvertent ignition. When the second grain is ignited the separation devices are automatically removed, fractured, or burned, but in such a manner that the

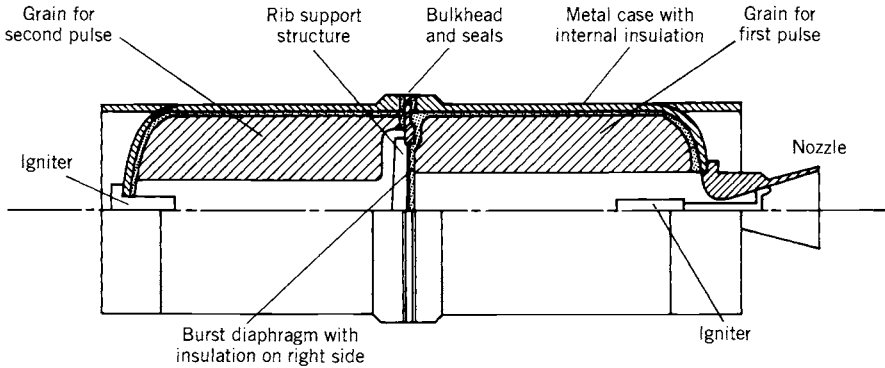


FIGURE 11-20. Simplified diagram of one concept of a two-pulse experimental rocket motor with two grains separated by a bulkhead. During the first pulse operation the metal diaphragm is supported by a spider-web-like structure made of high temperature material. Upon ignition of the second stage, the scored diaphragm is loaded in the other direction; it breaks and its leaves peel back. The bulkhead opening has a much larger area than the nozzle throat.

fragments of hardware pieces will not plug the nozzle or damage the insulation (see Refs. 11-18 and 11-19).

Slivers

Any remaining unburnt propellant is known as slivers. Figure 11-5 and the figure in Problem 11-6 show small slivers or pieces of unburnt propellant remaining at the periphery of the grain, because the pressure went below the deflagration limit (see Ref. 11-20). About 25 years ago grain designs had 2 to 7% propellant slivers; this useless material caused a reduction in propellant mass fraction and vehicle mass ratio. The technology of grain design has advanced so that there are almost no slivers (usually less than 1%). If slivers were to occur in a new unusual grain design, the designer would try to replace the sliver volume with lower-density insulator, which gives less of a mass ratio penalty than the higher-density propellant residue. This is shown in Fig. 11-17.

11.4. PROPELLANT GRAIN STRESS AND STRAIN

The objective of stress analysis of rocket motors is to design the configuration of the grain, the liners, or the grain support in such a way that excessive stresses or excessive strains will not occur and so that there will be no failure. Static and dynamic loads and stresses are imposed on the propellant grains during manufacture, transportation, storage, and operation. Structurally, a rocket motor is a thin shell of revolution (motor case) almost completely filled with a vis-

coelastic material, the propellant, which usually accounts for 80 to 94% of the motor mass. Propellant has some mechanical properties that are not found in ordinary structural materials and these have received relatively little study. The viscoelastic nature of solid propellant is time–history dependent and the material accumulates damage from repeated stresses; this is known as the *cumulative-damage phenomenon*.

The most common *failure modes* are:

1. Surface cracks are formed when the surface strain is excessive. They open up new additional burning surfaces and this in turn causes the chamber pressure as well as the thrust to be increased. The higher, shorter duration thrust will cause the vehicle to fly a different trajectory and this may cause the mission objective to be missed. With many cracks or deep cracks, the case becomes overpressurized and will fail. The limiting strain depends on the stress level, grain geometry, temperature, propellant age, load history, and the sizes of flaws or voids. At a high strain rate, deeper, more highly branched cracks are more readily formed than at a lower strain rate (see Ref. 11–9).
2. The bond at the grain periphery is broken and an unbonded area or gap can form next to the liner, insulator, or case. As the grain surface regresses, a part of the unbonded area will become exposed to the hot, high-pressure combustion gases, and then suddenly the burning area is increased by the unbonded area.

Other failure modes, such as an excessively high ambient grain temperature causing a large reduction in the physical strength properties, ultimately result in grain cracks and/or debonding. Air bubbles, porosity, or uneven density can locally reduce the propellant strength sufficiently to cause failure, again by cracks or debonds. Other failure modes are excessive deformations of the grain (e.g., slump of large grains can restrict the port area) and involuntary ignition due to the heat absorbed by the viscoelastic propellant from excessive mechanical vibration (e.g., prolonged bouncing during transport).

If the grain has a large number of small cracks or a few deep cracks or large areas of unbonding prior to firing, the burning area will increase, often progressively and unpredictably, and the resulting higher pressure will almost always cause the case to burst. A few small cracks or minor unbonded areas will usually not impede satisfactory motor operation.

Material Characterization

Before a structural analysis can be performed it is necessary to understand the materials and obtain data on their properties. The grain materials (propellant, insulator, and liner) are rubber-like materials that are nearly incompressible. They all have a *bulk modulus in compression* of at least 1400 MPa or about 200,000 psi in their original state (undamaged). Since there are very few voids

in a properly made propellant (much less than 1%), its compression strain is low. However, the propellant is easily damaged by applied tension and shear loads. If the strength of propellant in tension and shear (typically between 50 and 1000 psi) is exceeded, the grain will be damaged or fail locally. Since grains are three-dimensional, all stresses are combined stresses and not pure compression stresses, and grains are thus easily damaged. This *damage* is due to a “dewetting” of the adhesion between individual solid particles and the binder in the propellant and appears initially as many small voids or porosity. Those very small holes or debonded areas next to or around the solid particles may initially be under vacuum, but they become larger with strain growth.

The propellant, liner, and insulator with a solid filler are viscoelastic materials. They show a nonlinear viscoelastic behavior, not a linear elastic behavior. This means that the maximum stress and maximum elongation or strain diminish each time a significant load is applied. The material becomes weaker and suffers some damage with each loading cycle or thermal stress application. The physical properties also change with the time rate of applying loads; for example, very fast pressurization actually gives a stronger material. Certain binders, such as hydroxyl-terminated polybutadiene (HTPB), give good elongation and a stronger propellant than other polymers used with the same percentage of binder. Therefore HTPB is a preferred binder today. The physical properties are also affected by the manufacturing process. For example, tensile specimens cut from the same conventionally cast grain of composite propellant can show 20 to 40% variation in the strength properties between samples of different orientations relative to the local casting slurry flow direction. Viscoelastic material properties change as a function of prior loading and damage history. They have the capability to reheat and recover partially following damage. Chemical deterioration will in time degrade the properties of many propellants. These phenomena make it difficult to characterize these materials and predict their behavior or physical properties in engineering terms.

Several kinds of laboratory tests on small samples are routinely performed today to determine the physical properties of these materials. (see Refs. 11–21 and 11–22). Simple tests, however, do not properly describe the complex nonlinear behavior. These laboratory tests are conducted under ideal conditions—mostly uniaxial stresses instead of complex three-dimensional stresses—with a uniform temperature instead of a thermal gradient and usually with no prior damage to the material. The application of laboratory test results to real structural analysis therefore involves several assumptions and empirical correction factors. The test data are transformed into derived parameters for determining safety margins and useful life, as described in Chapter 9 of Ref. 11–1. There is no complete agreement on how best to characterize these materials. Nevertheless, laboratory tests provide useful information and several are described below.

The most common test is a simple *uniaxial tensile test* at constant strain rate. One set of results is shown in Fig. 11–21. The test is commonly used for manufacturing quality control, propellant development, and determining fail-

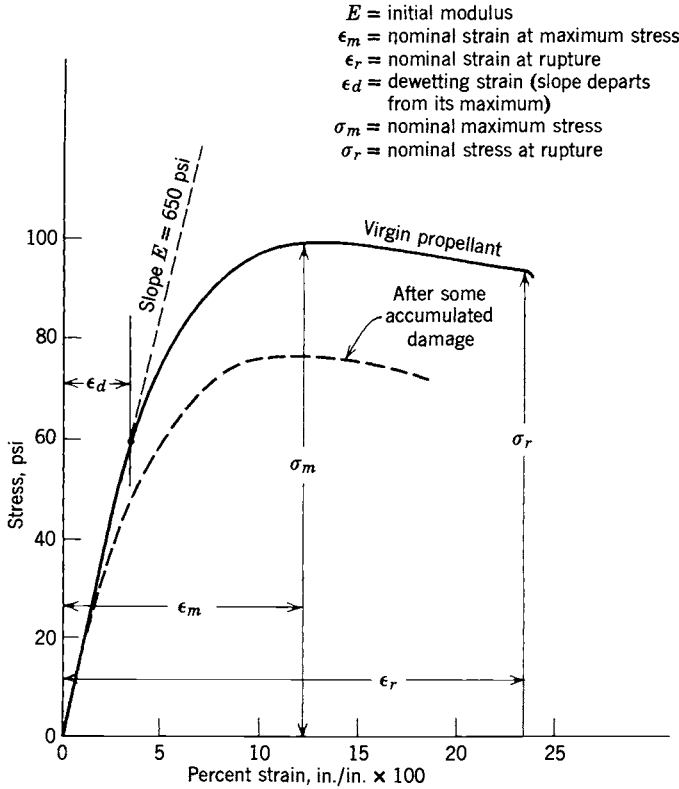


FIGURE 11-21. Stress-strain curves for a typical composite-type solid propellant showing the effect of cumulative damage. The maximum stress σ_m is higher than the rupture stress σ_r , of the tensile test sample.

ure criteria. Once the sample has been loaded, unloaded, and restressed several times, the damage to the material changes its response and properties as shown by the dashed curve in Fig. 11-21.

The dewetting strain is, by definition, the strain (and corresponding maximum stress) where incipient failure of the interface bonds between small solid oxidizer crystals and the rubbery binder occurs. The dewetting stress is analogous to the yield point in elastic materials, because this is when internal material damage begins to happen. The slope E , the modulus at low strain, is not ordinarily used in design, but is often used as a quality control parameter. Data from several such uniaxial tests at different temperatures can then be manipulated to arrive at allowable stresses, permissible safe strains, and a derived artificial modulus, as described later. Once a case-bonded grain has been cooled down from its casting temperature it will have shrunk and be under multidirectional strain. Samples cut from different parts of a temperature-cycled grain will usually give different tensile test results.

Biaxial strength tests are also performed frequently in the laboratory. One type is described in Ref. 11–21. Meaningful three-dimensional stress tests are difficult to perform in the laboratory and are usually not done. There are other sample tests that give information about propellant behavior, such as strain endurance tests to obtain the levels of strain at which the propellant has long endurance and does not suffer significant damage, tests at constant stress levels, fracture tests of samples with known cracks or defects, tensile tests under simulated chamber pressure, or tests to measure the thermal coefficient of expansion. Peel tests of the adhesive bonds of propellants to liners or insulators are very common and their failures are discussed in Ref 11–22. The application and interpretation of all these tests depend on the stress conditions in the grain and company preferences. In addition, strain or stress measurements are made occasionally on full-scale, experimental, flight-weight motors using special embedded sensors. Care must be taken that the implanting of these sensors into the grain will not disturb the local stress–strain distribution, which would lead to erroneous measurements.

The maximum failure stresses of most propellants are relatively low compared to those of plastic materials. Typical values range from about 0.25 to 8 MPa or about 40 to about 1200 psi, with average values between 50 and 300 psi, and elongations range from 4 to 250%, depending on the specific propellant, its temperature, and its stress history. Table 11–5 shows properties for a relatively strong propellant. Some double-base propellants and binder-rich composite propellants can withstand higher stresses (up to about 32 MPa or 4600 psi). The pressure and the strain rate have a major influence on the physical properties. Tensile tests performed at chamber pressure give higher strength than those done at atmospheric pressure, in some cases by a factor of 2 or more. High strain rates (sudden-start pressurization) can also improve the propellant properties temporarily.

The strength properties of the grain material are commonly determined over a range of propellant temperatures. For air-launched missiles these limits are

TABLE 11–5. Range of Tensile Properties of Reduced Smoke Composite Propellant for a Tactical Missile^a

	Temperature (°F)		
	158	77	–40
Maximum stress (psi)	137–152	198–224	555–633
Modulus (psi)	262–320	420–483	5120–6170
Strain at maximum stress/strain and at ultimate stress (%)	54/55–65/66	56/57–64/66	46/55–59/63

^aPolybutadiene binder with reduced aluminum and ammonium perchlorate; data are from four different 5-gallon mixes.

Source: Data taken with permission of the AIAA from Ref. 11–23.

wide, with -65°F and $+160^{\circ}\text{F}$ or 219 K and 344 K often being the lower and upper extremes expected during motor exposure. Propellant grains must be strong enough and have elongation capability sufficient to meet the high stress concentrations present during shrinkage at low temperature and also under the dynamic load conditions of ignition and motor operation. The mechanical properties (strength, elongation) can be increased by increasing the percent of binder material in the propellant, but at a reduction in performance.

Structural Design

The structural analysis of a typical case-bonded grain has to consider not only the grain itself but also the liner, insulator, and case, which interact structurally with the propellant grain under various loading conditions (see Chapter 9 or Ref. 11-1). The need to obtain strong bonds between the propellant and the liner, the liner and the insulator, or the insulator and the case is usually satisfied by using properly selected materials and manufacturing procedures to assure a good set of bonds. Liners are usually flexible and can accept large strains without failure, and the vehicle loads can be transmitted from the case (which is usually part of the vehicle structure) into the propellant.

When the propellant is cured (heated in an oven), it is assumed to have uniform internal temperature and to be free of thermal stresses. As the grain cools and shrinks after cure and reaches an equilibrium uniform ambient temperature (say, from -40 to $+75^{\circ}\text{F}$), the propellant experiences internal stresses and strains which can be relatively large at low temperature. The stresses are increased because the case material usually has a thermal coefficient of expansion that is smaller than that of the propellant by an order of magnitude. The stress-free temperature range of a propellant can be changed by curing the motor under pressure. Since this usually reduces the stresses at ambient temperature extremes, this pressure cure is now being used more commonly.

The structural analysis begins when all loads can be identified and quantified. Table 11-6 lists the typical loads that are experienced by a solid propellant motor during its life cycle and some of the failures they can induce. Some of these loads are unique to specific applications. The loads and the timing of these loads during the life cycle of a solid propellant rocket motor have to be analyzed for each application and each motor. They depend on the motor design and use. Although ignition and high accelerations (e.g., impact on a motor that falls off a truck) usually cause high stresses and strains, they may not always be the critical loads. The stresses induced by ambient environmental temperature cycling or gravity slumps are often relatively small; however, they are additive to stresses caused by other loads and thus can be critical. A space motor that is to be fired within a few months after manufacture presents a different problem than a tactical motor that is to be transported, temperature cycled, and vibrated for a long time, and this is different yet from a large-diameter ballistic missile motor that sits in a temperature-conditioned silo for more than 10 years.

TABLE 11-6. Summary of Loads and Likely Failure Modes in Case-Bonded Rocket Motors

Load Source	Description of Load and Critical Stress Area
1. Cool-down during manufacture after hot cure	Temperature differential across case and grain; tension and compression stresses on grain surfaces; hot grain, cool case
2. Thermal cycling during storage or transport	Alternative hot and cold environment; critical condition is with cold grain, hot case; two critical areas: bond-line tensile stress (tearing), inner-bore surface cracking
3. Improper handling and transport vibrations	Shock and vibration, 5 to 30g ₀ forces during road transport at 5 to 300 Hz (5 to 2500 Hz for external aircraft carry) for hours or days; critical failure: grain fracture or grain debonding
4. Ignition shock/pressure loading	Case expands and grain compresses; axial pressure differential is severe with end-burning grains; critical areas; fracture and debonding at grain periphery
5. Friction of internal gas flow in cavity	Axially rearward force on grain
6. Launch and axial flight acceleration	Inertial load mostly axial; shear stress at bond line; slump deformation in large motors can reduce port diameter
7. Flight maneuvers (e.g., antimissile rocket)	High side accelerations cause unsymmetrical stress distribution; can result in debonding or cracks
8. Centrifugal forces in spin-stabilized projectiles/missiles	High strain at inner burning surfaces; cracks will form
9. Gravity slump during storage; only in large motors	Stresses and deformation in perforation can be minimized by rotating the motor periodically; port area can be reduced by slump
10. External air friction when case is also the vehicle's skin	Heating of propellant, liner and insulators will lower their strengths causing premature failure. Induces thermal stresses

Furthermore, the structural analysis requires a knowledge of the material characteristics and *failure criteria*: namely, the maximum stress and strains that can safely be accepted by the propellant under various conditions. The failure criteria are derived from cumulative damage tests, classical failure theories, actual motor failures, and fracture mechanics. This analysis may be an iterative

analysis, because the materials and geometry need to be changed if analysis shows that the desired margins of safety are exceeded.

Ideally, the analysis would be based on a nonlinear viscoelastic stress theory; however, such an approach is still being developed and is not yet reliable (see Ref. 11-1). An analysis based on a viscoelastic material behavior is feasible, relatively complex, and requires material property data that are difficult to obtain and uncertain in value. Most structural analyses today are based on an elastic material model; it is relatively simple and many two- and three-dimensional finite element analysis computer programs of this approach are available at rocket motor manufacturing companies. Admittedly, this theory does not fit all the facts, but with some empirical corrections it has given approximate answers to many structural grain design problems. An example of a two-dimensional finite element grid from a computer output is shown in Fig. 11-22 for a segment of a grain using an elastic model (see Refs. 11-24 and 11-25).

With elastic materials the stress is essentially proportional to strain and independent of time; when the load is removed, the material returns to its original condition. Neither of these propositions is valid for grains or their propellant materials. In viscoelastic material a time-related dependency exists between stresses and strains; the relationship is not linear and is influenced by the rate of strain. The stresses are not one-dimensional as many laboratory tests are, but three-dimensional, which are more difficult to visualize. When the load is removed, the grain does not return to its exact original position. References 11-26 and 11-27 and Chapters 9 and 10 of Ref. 11-1 discuss three-dimensional analysis techniques and viscoelastic design. A satisfactory analysis technique has yet to be developed to predict the influence of cumulative damage.

Various techniques have been used to compensate for the nonelastic behavior by using allowable stresses that have been degraded for nonlinear effects and/or an effective modulus that uses a complex approximation based on laboratory strain test data. Many use a modified modulus (maximum stress-strain at maximum stress or σ_m/ϵ_m in Fig. 11-21) called the *stress relaxation modulus* E_R in a master curve against temperature-compensated time to failure, as shown in Fig. 11-23. It is constructed from data collected from a series of uniaxial tests at constant strain rate (typically, 3 to 5%) performed at different temperatures (typically -55 to $+43^\circ\text{C}$). The shifted temperature T_s/T is shown in the inset on the upper right for 3% strain rate and sample tests taken at different temperatures. The factor λ in the ordinate corrects for the necking down of the tension sample during test. The small inset in this figure explains the correction for temperature that is applied to the reduced time to failure. The empirical time-temperature shift factor a_T is set to zero at ambient temperatures (25°C or 77°F) and graphically shifted for higher and lower temperatures. The master curve then provides time-dependent stress-strain data to calculate the response of the propellant for structural analysis (see Ref. 11-21 and Chapter 9 of Ref. 11-1).

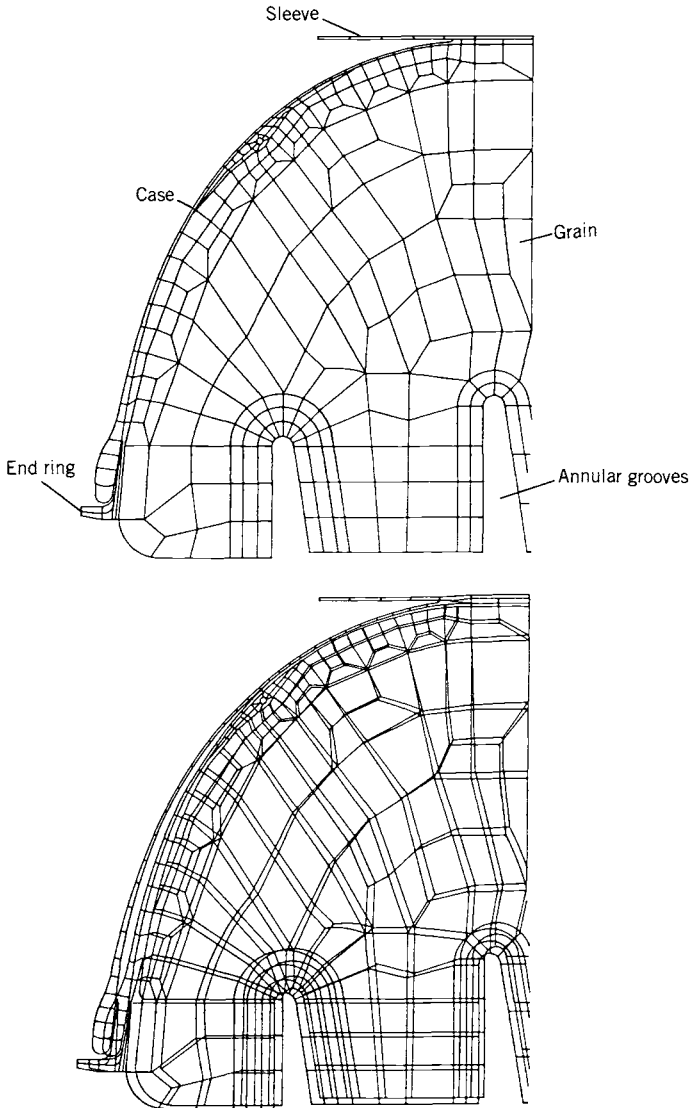


FIGURE 11-22. Finite element analysis grid of the forward end of a cast grain in a filament-wound plastic case. The grain has an internal tube and annular grooves. The top diagram shows the model grid elements and the bottom shows one calculated strain or deformation condition. (Reprinted with permission from A. Turchot, Chapter 10 of Ref. 11-1).

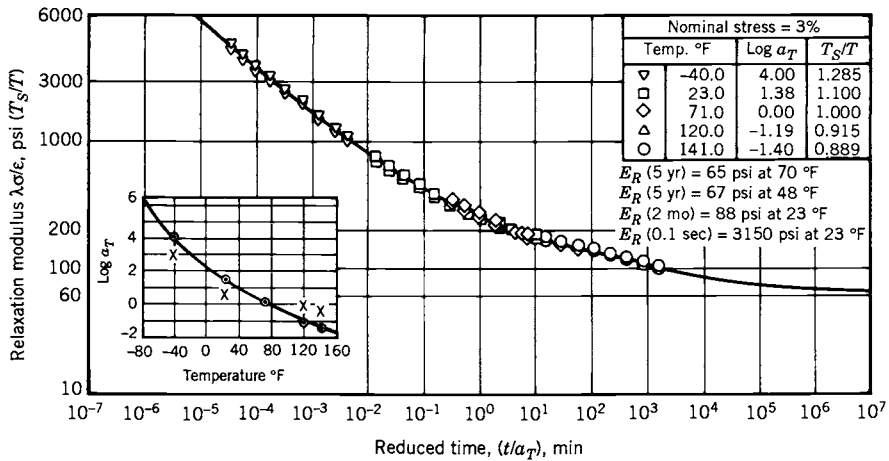


FIGURE 11-23. This stress-relaxation modulus master curve for a particular composite solid propellant is constructed from manipulated data taken from a number of uniaxial tensile tests at constant strain rate but different temperatures. (Reproduced with permission of United Technologies Corp., Chemical Systems from Ref. 11-27.)

Usually, several different grain loading and operating conditions need to be analyzed. Such a structural analysis is useful for identifying locations of maximum stress or strain and to any structural members or grain sectors that are too weak or too heavy, but these analyses have not always been successful. The choice of the best analysis tool and the best pseudo-viscoelastic compensation factors will depend on the experience of the stress analyst, the specific motor design conditions, the complexity of the motor, the geometry, and suitable, available, valid propellant property data.

In a case-bonded motor, special provision is required to reduce the stress concentrations at the grain ends where the case and grain interface, especially for motors expected to operate satisfactorily over a wide range of temperatures. Basically, the high stresses arise from two primary sources. First, the physical properties, including the coefficient of thermal expansion of the case material and the propellant, are grossly dissimilar. The coefficient of expansion of a typical solid propellant is 1.0×10^{-4} m/m-K, which is five times as great as that of a steel motor case. Secondly, the aft-end and head-end geometries at the grain-case juncture often present a discontinuity, with the grain stress theoretically approaching infinity. Actually, finite stresses exist because viscoplastic deformations do occur in the propellant, the liner, and the case insulation. Calculating the stress in a given case-grain termination arrangement is usually impractical, and designers rely on approximations supported by empirical data.

For simple cylindrical grains the highest stresses usually occur at the outer and inner surfaces, at discontinuities such as the bond surface termination point, or at stress concentration locations, such as sharp radii at the roots or

tips of star or wagonwheel perforations, as shown in Fig. 11–16. Figure 11–24 shows a *stress relief flap*, sometimes called a *boot*, a device to reduce local stresses. It is usually an area on the outside of the grain near its aft end (and sometimes also its forward end), where the liner material is not sticky but has a non-adhesive coating that permits the grain to shrink away from the wall. It allows for a reduction of the grain at the bond termination point. It moves the location of highest stress into the liner or the insulation at the flap termination or hinge. Normally, the liner and insulation are much stronger and tougher than the propellant.

Parametric studies of propellant and case-bond stresses of a typical grain–case termination design (Fig. 11–24) reveal the following:

1. Flap length is less significant than the thickness of the insulation or the separate flap boot, if one is used, in controlling the local level of stresses at the grain–case termination.
2. The distribution of stresses at the grain–case termination is sensitive to the local geometry; the level of stress at the case bond increases with web fraction and length-to-diameter ratio under loading by internal pressure and thermal shrinkage.
3. As the L/D and web fraction increase, the inner-bore hoop stress and the radial stress at the grain–case bond increase more rapidly than does the

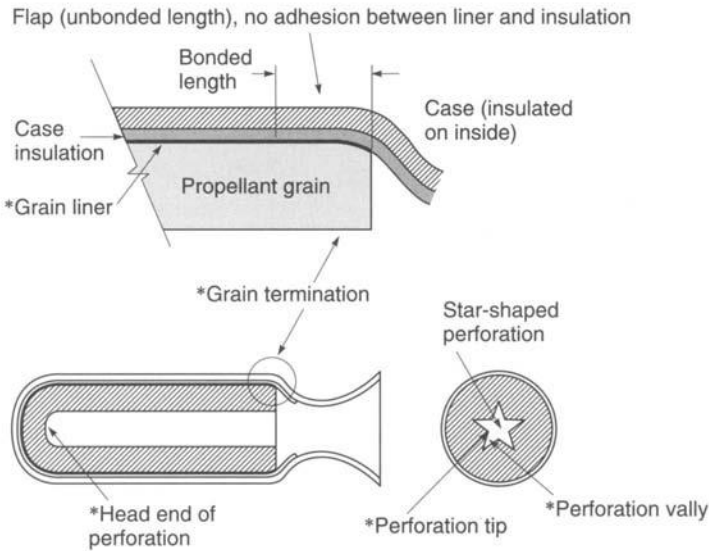


FIGURE 11–24. The asterisks in the bottom simplified diagram denote potentially critical failure areas. The top sketch is an enlargement of the aft termination region of the grain and shows a boot or stress relief flap.

grain–case termination stress under internal pressure and thermal shrinkage loads.

4. The radial case-bond stress level at the grain–case termination is much larger than the case-bond shear stress under axial acceleration loading as well as under internal pressure and thermal shrinkage loading.

Aging of propellants in rocket motors refers to their deterioration in the physical properties with time. It is caused by the *cumulative damage* done to the grain (such as by thermal cycling, and load applications) during storage, handling, or transport. It can also be caused by chemical changes with time, such as the gradual depletion (evaporation) of certain liquid plasticizers or moisture absorption. The ability to carry stress or to allow elongation in propellants diminishes with cumulative damage. The *aging limit* is the estimated time when the motor is no longer able to perform its operation reliably or safely (see Refs. 11–28 and 11–29). Depending on the propellant and the grain design, this age limit or motor life can be between 8 and 25 years. Before this limit is reached, the motor should be deactivated and have its propellant removed and replaced. This refurbishing of propellant is routinely done on larger and more expensive rocket motors in the military inventory.

With small tactical rocket motors the aging limit is usually determined by full-scale motor-firing tests at various time periods after manufacture, say 2 or 3 years and with an extrapolation to longer time periods. Accelerated temperature aging (more severe thermal cycles) and accelerated mechanical pulse loads and overstressing are often used to reduce the time needed for these tests. For large rocket motors, which are more expensive, the number of full-scale tests has to be relatively small, and aging criteria are then developed from structural analysis, laboratory tests, and subscale motor tests.

Many of the early grains were *cartridge loaded* and kept the grain isolated from the motor case to minimize the interrelation of the case and the grain stresses and strains resulting from thermal expansion. Also, upon pressurization the case would expand, but the grain would shrink. The case-bonded grain presents a far more complex problem in stress analysis. With the propellant grain bonded firmly to the case, being a semirubbery and relatively weak material, it is forced to respond to case strains. As a result, several critically stressed areas exist in every case-bonded motor design; some are shown with an asterisk in Fig. 11–24.

The varying nature of the stress analysis problem is brought about by the physical character of propellant; in general terms, solid propellant is relatively weak in tension and shear, is semielastic, grows softer and weaker at elevated temperatures, becomes hard and brittle at low temperatures, readily absorbs and stores energy upon being vibrated, degrades physically during long-term storage because of decomposition and chemical or crystalline changes, and accumulates structural damage under load, including cyclic load. This last phenomenon is shown graphically in Fig. 11–25 and is particularly important in the analysis of motors that are to have a long shelf-life (more than 10 years).

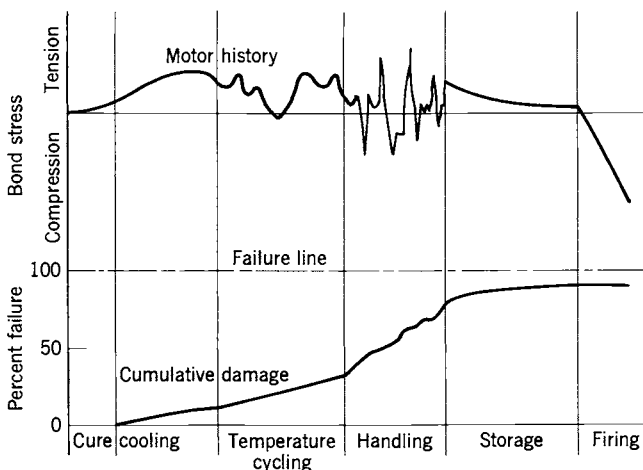


FIGURE 11-25. Representation of the progress in cumulative damage to the bond between the grain and the case in a case-bonded rocket motor experiencing a hypothetical stress history. (Adapted from Ref. 11-30.)

No a priori reason is known for materials to exhibit *cumulative damage*, but propellants and their bond to case material exhibit this trait even under constant load, as shown in Fig. 11-26. Valid theories and analytical methods applicable to cumulative damage include a consideration of both the stress-strain history and the loading path (the material effected). The most important environmental variables affecting the shelf life of a motor are time, temperature

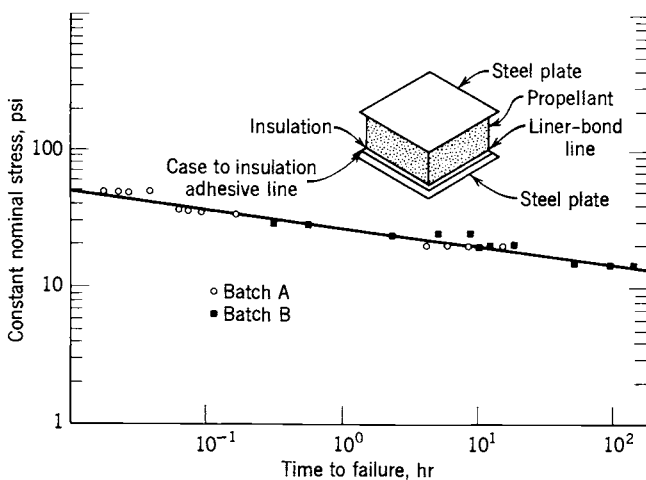


FIGURE 11-26. Time dependent reduction of the propellant-liner-insulator bond strength when subjected to constant load at 77°F. (From Ref. 11-31.)

cycles, propellant mass, stress (gravity forces for large motors), and shock and vibration. Failure due to cumulative damage usually appears as cracks in the face of the perforation or as local “unbonds” in case-bonded motors.

The strength of most propellants is sensitive to the rate of strain; in effect they appear to become more brittle at a given temperature as the strain rate is increased, a physical trait that is important during the ignition process.

11.5. ATTITUDE CONTROL AND SIDE MANEUVERS WITH SOLID PROPELLANT ROCKET MOTORS

A clever attitude control (also called reaction control) system with solid propellants is used on some ballistic missiles. Its hot reaction gas has a low enough temperature so that uncooled hardware can be used for long durations. Ammonium nitrate composite propellant (mentioned as gas generator propellants in Tables 12–1 and 12–2) or a propellant consisting of a nitramine (RDX or HMX, described in Chapter 12) with a polymer binding are suitable. The version shown schematically in Fig. 11–27 provides pitch and yaw control; hot gas flows continuously through insulated manifolds, open hot-gas valves, and all four nozzles. When one of these valves is closed, it causes an unbalance of gas flow and produces a side force. To keep things simple, the four roll-control thrusters have been deleted from this figure.

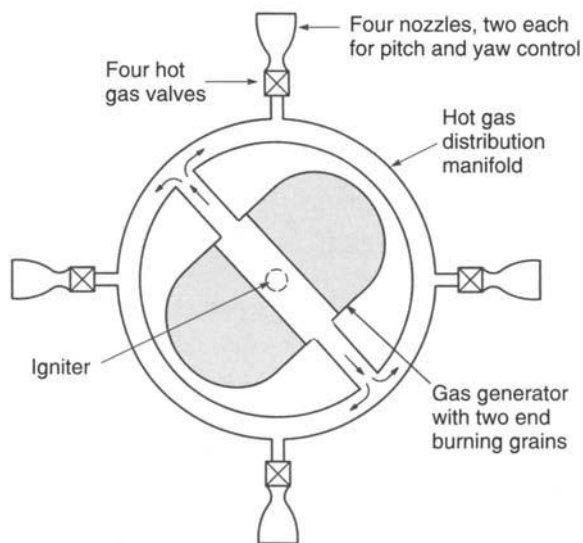


FIGURE 11–27. Simplified diagram of a rocket attitude control system using solid propellant. All four valves are normally open and gas flows equally through all nozzles.

With this type of attitude control system it is possible to achieve variable duration thrust pulsing operations and random pitch, yaw, and roll maneuvers. It is competitive with multi-thruster liquid propellant attitude control systems. The solid propellant versions are usually heavier, because they have heavy insulated hardware and require more propellant (for continuous gas flow), whereas the liquid version is operated only when attitude control motions are required.

A similar approach with hot gas valves applies to upper stages of interceptor vehicles used for missile defense; there is little time available for maneuvers of the upper stage to reach the incoming missile or aircraft and therefore the burning durations are usually short. The solid propellant gas temperatures are higher than with gas generators (typically 1260°C or 2300°F), but lower than with typical composite propellants (3050 K or 5500°F), and this allows the valves and manifolds to be made of high-temperature material (such as rhenium or carbon). In addition to attitude control, the system provides a substantial side force or divert thrust. It displaces the flight path laterally. Figure 11–28 shows such a system. Since all hot-gas valves are normally open, a valve has to be closed to obtain a thrust force as explained in the previous figure. The attitude control system provides pitch, yaw, and roll control to stabilize the vehicle during its flight, to orient the divert nozzle into the desired direction, and sometimes to orient the seeker (at the front of the vehicle) toward the target.

PROBLEMS

1. What is the ratio of the burning area to the nozzle area for a solid propellant motor with these characteristics?

Propellant specific gravity	1.71
Chamber pressure	14 MPa
Burning rate	38 mm/sec
Temperature sensitivity σ_p	0.007 (K)^{-1}
Specific heat ratio	1.27
Chamber gas temperature	2220 K
Molecular mass	23 kg/kg-mol
Burning rate exponent n	0.3

2. Plot the burning rate against chamber pressure for the motor in Problem 1 using Eq. 11–3 between chamber pressures of 11 and 20 MPa.
3. What would the area ratio A_b/A_t in Problem 1 be if the pressure were increased by 10%? (Use curve from Problem 2.)
4. Design a simple rocket motor for the conditions given in Problems 1 and 2 for a thrust of 5000 N and a duration of 15 sec. Determine principal dimensions and approximate weight.

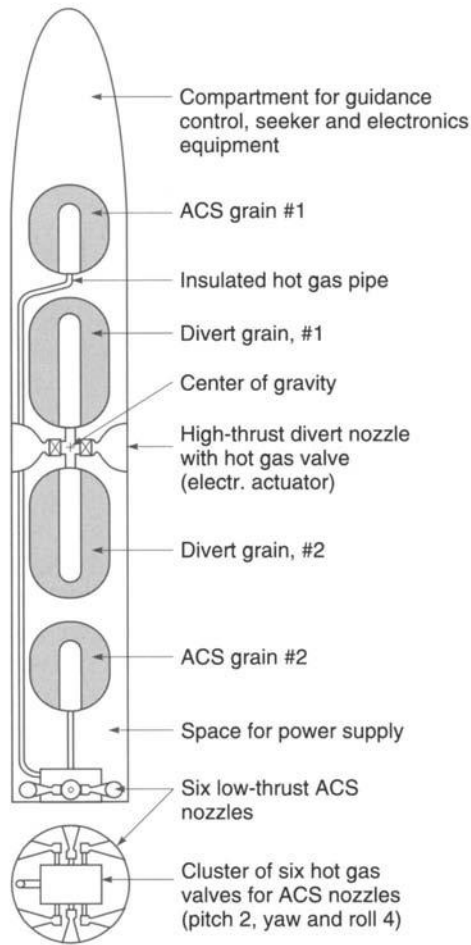
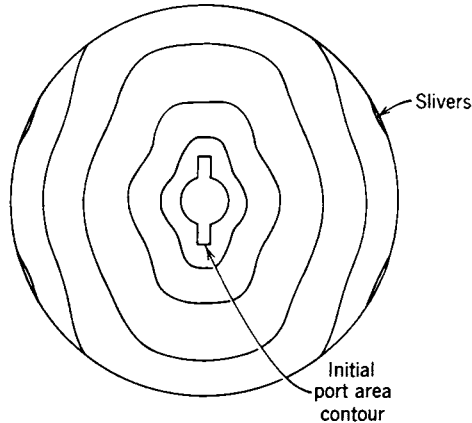


FIGURE 11-28. Simplified schematic diagram of two propulsion systems for one type of maneuverable upper stage of an interceptor missile. The side or divert forces are relatively large and go essentially through the center of gravity (CG) of the upper stage vehicle. To minimize the CG travel two grains are above and two grains are below the CG. Each nozzle has its own hot gas valve, which is normally open and can be pulsed. The attitude control system (ACS) is fed from the reaction gas of two grains and has six small nozzles.

- For the Orbus-6 rocket motor described in Table 11-3 determine the total impulse-to-weight ratio, the thrust-to-weight ratio, and the acceleration at start and burnout if the vehicle inert mass and the payload come to about 6000 lbm. Use burn time from Table 11-3 and assume $g \approx 32.2 \text{ ft/sec}^2$.
- For a cylindrical two-dimensional grain with two slots the burning progresses in finite time intervals approximately as shown by the successive burn surface contours in the drawing on the next page. Draw a similar set of progressive burning surfaces

for any one configuration shown in Figure 11-16 and one shown in Figure 11-17, and draw an approximate thrust-time curve from these plots, indicating the locations where slivers will remain. Assume the propellant has a low value of n and thus the motor experiences little change in burning rate with chamber pressure.



7. Explain the significance of the web fraction, the volumetric loading ratio, and the L/D ratio in terms of vehicle performance and design influence.
8. The partial differential equations 11-4 and 11-5 express the influence of temperature on the burning of a solid propellant. Explain how a set of tests should be set up and exactly what should be measured in order to determine these coefficients over a range of operating conditions.
9. What would be the likely change in r , I_s , p_1 , F , t_b , and I_t if the three rocket motors described in Table 11-3 were fired with the grain 100°F cooler than the data shown in the table? Assume typical average temperature effects.
10. A newly designed case-bonded rocket motor with a simple end-burning grain failed and exploded on its first test. The motor worked well for about 20% of its burn time, when the record showed a rapid rise in chamber pressure. It was well conditioned at room temperature before firing and the inspection records did not show any flaws or voids in the grain. Make a list of possible causes for this failure and suggestions on what to do in each case to avoid a repetition of the failure.
11. Derive Eq. 11-7. (*Hint*: First derive π_K by differentiating Eq. 11-3 with respect to temperature.) *Note*: This relation does not fit all the experimental data fully because there are other variables besides n that have a mild influence. For a more complex approach, see Ref. 11-32.
12. What will be the percent change in nominal values of A_t , r , I_s , T_0 , t_b , A_b/A_t and the nozzle throat heat transfer rate, if the Orbus-6 rocket motor listed in Table 11-3 is to be downgraded in thrust for a particular flight by 15% by substituting a new nozzle with a larger nozzle throat area but the same nozzle exit area? The propellants, grain, insulation, and igniter will be the same.

13. What would be the new values of I_t , I_s , p_1 , F , t_b , and r for the first stage of the Minuteman rocket motor described in Table 11-3, if the motor were fired at sea level with the grain temperature 20°F hotter than the data shown. Use only data from this table.

Answers: $I_t = 10,240,000$ lbf-sec, $I_s = 224$ sec, $p_1 = 796$ psia, $F = 1.99 \times 10^5$ lbf, $t_b = 51.5$ sec, $r = 0.338$ in./sec.

SYMBOLS

a	burning rate constant, also called temperature coefficient
A_b	solid propellant burning area, m^2 (ft^2)
A_p	port area (flow area of gases inside grain cavity or between and around propellant grains), m^2 (ft^2)
A_t	nozzle throat cross-sectional area, m^2 (ft^2)
b	web thickness, m (in.)
b_f	web fraction, or web thickness-to-radius ratio
c	effective exhaust velocity, m/sec (ft/sec)
c^*	characteristic exhaust velocity, m/sec (ft/sec)
c_p	specific heat of gas, kcal/kg-K
c_s	specific heat of solid, kcal/kg-K
C_F	thrust coefficient
D	diameter, m (ft)
E_R	relaxation modulus, MPa (psi)
F	thrust, N (lbf)
\bar{F}	average thrust, N (lbf)
g_0	acceleration due to gravity at sea level, 9.8066 m/sec ² (32.2 ft/sec ²)
G	mass flow rate, kg-m ² /sec
h	enthalpy per unit mass, J/kg or Btu/lbm
I_s	specific impulse, sec
I_t	total impulse, N-sec (lbf-sec)
k	specific heat ratio
K	ratio of burning surface to throat area, A_b/A_t
L	length, m
m	mass, kg
\dot{m}	mass flow rate, kg/sec
n	burning rate exponent
p	pressure, MPa (lbf/in. ²)
p_1	chamber pressure, MPa (lbf/in. ²)
Pr	Prandtl number, $\mu c_p/\kappa$
r	propellant burning rate (velocity of consumption), m/sec or mm/sec or in./sec
R	gas constant, J/kg-K
t	time, sec
t_a	action time, sec

t_b	burn time, sec
T	absolute temperature, K(R)
v_2	theoretical exhaust velocity, m/sec (ft/sec)
V_b	propellant volume, m^3 (ft^3)
V_c	chamber volume, m^3 (ft^3)
V_f	volumetric loading fraction, %
w	total effective propellant weight, N (lbf)
w_G	total loaded rocket weight, or gross weight, N (lbf)
\dot{w}	weight rate of flow, N/sec (lbf/sec)

Greek Letters

α	heat transfer factor
β	constant
δ	partial derivative
ϵ	elongation or strain
κ	conductivity
μ	viscosity
π_K	temperature sensitivity coefficient of pressure, $K^{-1}(R^{-1})$
ρ	density, kg/m^3 (lbm/ft^3)
σ	stress, N/cm^2 (psi)
σ_p	temperature sensitivity coefficient of burning rate, $K^{-1}(R^{-1})$
ζ	propellant mass fraction

Subscripts

b	solid propellant burning conditions
p	pressure or propellant or port cavity
t	throat conditions
0	initial or reference condition
1	chamber condition
2	nozzle exit condition

REFERENCES

- 11-1. P. R. Evans, "Composite Motor Case Design," Chapter 4A; H. Badham and G. P. Thorp, "Considerations for Designers of Cases for Small Solid Propellant Rocket Motors," Chapter 6; B. Zeller, "Solid Propellant Grain Design," Chapter 8; D. I. Thrasher, "State of the Art of Solid Propellant Rocket Motor Grain Design in the United States," Chapter 9; and A. Truchot, "Design and Analysis of Rocket Motor Internal Insulation," Chapter 10; all of *Design Methods in Solid Propellant Rocket Motors*, AGARD Lecture Series 150, Revised Version, 1988.

- 11-2. N. Eisenreich, H. P. Kugler, and F. Sinn, "An Optical System for Measuring Burning Rates of Solid Propellants," *Propellants, Explosives, Pyrotechnics*, Vol. 12, 1987, pp. 78-80.
- 11-3. N. Kubota, "Survey of Rocket Propellants and their Combustion Characteristics," Chapter 1; and M. K. Rázdán and K. K. Kuo, "Erosive Burning of Solid Propellants," Chapter 10; in K. K. Kuo and M. Summerfield (Eds.), *Fundamentals of Solid Propellant Combustion*, Volume 90 in series on *Progress in Astronautics and Aeronautics*, American Institute of Aeronautics and Astronautics, New York, 1984, 891 pages.
- 11-4. S. D. Heister and R. J. Davis, "Predicting Burning Time Variations in Solid Rocket Motors," *Journal of Propulsion and Power*, Vol. 8, No. 3, May-June 1992.
- 11-5. M. K. King, "Erosive Burning of Solid Propellants," *Journal of Propulsion and Power*, Vol. 9, No. 6, November-December 1993.
- 11-6. J. M. Lenoir and G. Robillard, "A Mathematical Method to Predict the Effects of Erosive Burning in Solid-propellant Rocket," *Sixth Symposium (International) on Combustion*, Reinhold, New York, 1957, pp. 663-667.
- 11-7. "Solid Propellant Selection and Characterization," *NASA SP-8064*, June 19971 (N72-13737).
- 11-8. M. S. Fuchs, A. Peretz, and Y. M. Timnat, "Parametric Study of Acceleration Effects on Burning Rates of Metallized Solid Propellants," *Journal of Spacecraft and Rockets*, Vol. 19, No. 6, November-December 1982, pp. 539-544.
- 11-9. K. K. Kuo, J. Moreci, and J. Mantzaras, "Modes of Crack Formation in Burning Solid Propellant," *Journal of Propulsion and Power*, Vol. 3, No. 1, January-February 1987, pp. 19-25.
- 11-10. M. T. Langhenry, "The Direct Effects of Strain on Burning Rates of Solid Propellants," *AIAA Paper 84-1436*, June 1984.
- 11-11. M. K. King, "Analytical Modeling of Effects of Wires on Solid Motor Ballistics," *Journal of Propulsion and Power*, Vol. 7, No. 3, May-June 1991, pp. 312-320.
- 11-12. "Solid Rocket Motor Performance Analysis and Prediction," *NASA SP-8039*, May 1971 (N72-18785).
- 11-13. E. M. Landsbaum, M. P. Salinas, and J. P. Leavy, "Specific Impulse Predictions of Solid Propellant Motors," *Journal of Spacecraft and Rockets*, Vol. 17, 1980, pp. 400-406.
- 11-14. R. Akiba and M. Kohno, "Experiments with Solid Rocket Technology in the Development of M-3SII," *Acta Astronautica*, Vol. 13, No. 6-7, 1986, pp. 349-361.
- 11-15. P. R. Zarda and D. J. Hartman, "Computer-Aided Propulsion Burn Analysis," *AIAA Paper 88-3342*, July 1988 (cavity geometry).
- 11-16. R. J. Hejl and S. D. Heister, "Solid Rocket Motor Grain Burnback Analysis Using Adaptive Grids," *Journal of Propulsion and Power*, Vol. 11, No. 5, September-October 1995.
- 11-17. W. H. Jolley, J. F. Hooper, P. R. Holton, and W. A. Bradfield, "Studies on Coning in End-Burning Rocket Motors," *Journal of Propulsion and Power*, Vol. 2, No. 2, May-June 1986, pp. 223-227.

- 11-18. S. Nishi, K. Fukuda, and N. Kubota, "Combustion Tests of Two-Stage Pulse Rocket Motors," *AIAA Paper 89-2426*, July 1989, 5 pages.
- 11-19. L. C. Carrier, T. Constantinou, P. G. Harris, and D. L. Smith, "Dual Interrupted Thrust Pulse Motor," *Journal of Propulsion and Power*, Vol. 3, No. 4, July-August 1987, pp. 308-312.
- 11-20. C. Bruno et al., "Experimental and Theoretical Burning of Rocket Propellant near the Pressure Deflagration Limit," *Acta Astronautica*, Vol. 12, No. 5, 1985, pp. 351-360.
- 11-21. F. N. Kelley, "Solid Propellant Mechanical Property Testing, Failure Criteria and Aging," Chapter 8 in C. Boyars and K. Klager (Eds.), *Propellant Manufacture Hazards and Testing*, Advances in Chemistry Series 88, American Chemical Society, Washington, DC, 1969.
- 11-22. T. L. Kuhlmann, R. L. Peeters, K. W. Bills, and D. D. Scheer, "Modified Maximum Principal Stress Criterion for Propellant Liner Bond Failures," *Journal of Propulsion and Power*, Vol. 3, No. 3, May-June 1987.
- 11-23. R. W. Magness and J. W. Gassaway, "Development of a High Performance Rocket Motor for the Tactical VT-1 Missile," *AIAA Paper 88-3325*, July 1988.
- 11-24. I-Shih Chang and M. J. Adams, "Three-Dimensional, Adaptive, Unstructured, Mesh Generation for Solid-Propellant Stress Analysis," *AIAA Paper 96-3256*, July 1996.
- 11-25. W. A. Cook, "Three-Dimensional Grain Stress Analysis Using the Finite Element Method," *AFRPL Report TT-71-51*, Thiokol Corp., April 1971 (AD725043).
- 11-26. G. Meili, G. Dubroca, M. Pasquier, and J. Thenpenier, "Nonlinear Viscoelastic Design of Case-Bonded Composite Modified Double Base Grains," *AIAA Paper 80-1177R*, July 1980, and S. Y. Ho and G. Care, "Modified Fracture Mechanics Approach in Structural Analysis of Solid-Rocket Motors," *Journal of Propulsion and Power*, Vol. 14, No. 4, July-August 1998.
- 11-27. P. G. Butts and R. N. Hammond, "IUS Propellant Development and Qualification," Paper presented at the 1983 JANNAF Propulsion Meeting, Monterey, February 1983, 13 pages.
- 11-28. A. G. Christianson et al., "HTPB Propellant Aging," *Journal of Spacecraft and Rockets*, Vol. 18, No. 3, May-June 1983.
- 11-29. D. I. Thrasher and J. H. Hildreth, "Structural Service Life Estimates for a Reduced Smoke Rocket Motor," *Journal of Spacecraft and Rockets*, Vol. 19, No. 6, November 1982, pp. 564-570.
- 11-30. S. W. Tsai (Ed.), *Introduction to Viscoelasticity*, Technomic Publishing Co., Stamford, CT, Conn., 1968.
- 11-31. J. D. Ferry, *Viscoelastic Properties of Polymers*, John Wiley & Sons, New York, 1970.
- 11-32. R. E. Hamke, M. T. Gaunce, and J. R. Osborn, "The Effect of Pressure Exponent on Temperature Sensitivity," *Acta Astronautica*, Vol. 15, Nos. 6 and 7, 1987, pp. 377-382.